AMERICAN SOCIETY FOR MICROBIOLOGY | Journal of Virology®

VIRUS-CELL INTERACTIONS

# Disruption of Stress Granule Formation by the Multifunctional Cricket Paralysis Virus 1A Protein

**Anthony Khong,[a] Craig H. Kerr,[a] Clarence H. L. Yeung,[a] Kathleen Keatings,[b] Arabinda Nayak,[c] Douglas W. Allan,[b] Eric Jan[a]**

Department of Biochemistry and Molecular Biology[a] and Department of Cellular and Physiological Sciences, University of British Columbia, Vancouver, BC, Canada[b]; University of California–San Francisco, Department of Microbiology and Immunology, San Francisco, California, USA[c]

**ABSTRACT** Stress granules (SGs) are cytosolic ribonucleoprotein aggregates that are induced during cellular stress. Several viruses modulate SG formation, suggesting that SGs have an impact on virus infection. However, the mechanisms and impact of modulating SG assembly in infected cells are not completely understood. In this study, we identify the dicistrovirus cricket paralysis virus 1A (CrPV-1A) protein that functions to inhibit SG assembly during infection. Moreover, besides inhibiting RNA interference, CrPV-1A also inhibits host transcription, which indirectly modulates SG assembly. Thus, CrPV-1A is a multifunctional protein. We identify a key R146A residue that is responsible for these effects, and mutant CrPV(R146A) virus infection is attenuated in *Drosophila melanogaster* S2 cells and adult fruit flies and results in increased SG formation. Treatment of CrPV(R146A)-infected cells with actinomycin D, which represses transcription, restores SG assembly suppression and viral yield. In summary, CrPV-1A modulates several cellular processes to generate a cellular environment that promotes viral translation and replication.

**IMPORTANCE** RNA viruses encode a limited set of viral proteins to modulate an array of cellular processes in order to facilitate viral replication and inhibit antiviral defenses. In this study, we identified a viral protein, called CrPV-1A, within the dicistrovirus cricket paralysis virus that can inhibit host transcription, modulate viral translation, and block a cellular process called stress granule assembly. We also identified a specific amino acid within CrPV-1A that is important for these cellular processes and that mutant viruses containing mutations of CrPV-1A attenuate virus infection. We also demonstrate that the CrPV-1A protein can also modulate cellular processes in human cells, suggesting that the mode of action of CrPV-1A is conserved. We propose that CrPV-1A is a multifunctional, versatile protein that creates a cellular environment in virus-infected cells that permits productive virus infection.

**KEYWORDS** stress granules, virus, dicistrovirus, RNA, transcription, *Drosophila*, cricket paralysis virus, insect viruses, translation

**Received** 3 September 2016 **Accepted** 15 December 2016

**Accepted manuscript posted online** 21 December 2016

**Citation** Khong A, Kerr CH, Yeung CHL, Keatings K, Nayak A, Allan DW, Jan E. 2017. Disruption of stress granule formation by the multifunctional cricket paralysis virus 1A protein. J Virol 91:e01779-16. https://doi.org/10.1128/JVI.01779-16.

**Editor** Anne E. Simon, University of Maryland



Address correspondence to Eric Jan, ej@mail.ubc.ca.

Stress granules (SGs) are nonmembranous aggregates of nontranslating ribonucleoproteins (mRNPs) that form when translation is limited due to cellular stress (1). SGs are important for cellular regulation; the assembly of SGs can affect mRNA localization, translation, and degradation, and the compartmentalization of some cellular proteins to SGs can affect signaling pathways such as apoptosis, mTOR, and innate immunity (1–6).

In general, SGs form through inhibiting overall translation, whereby stalled translation initiation complexes (i.e., nontranslating mRNPs) aggregate via a mechanism that is poorly understood. Classical induction of SG formation occurs via eIF2$\alpha$ phosphorylation, which inhibits a critical step in translation initiation and is triggered in response

to environmental stresses by eIF2$\alpha$ kinases (7, 8). SG formation can also be triggered in an eIF2$\alpha$-independent manner. For example, the addition of pateamine A (PatA) to cells also triggers SG formation by modulating eIF4A helicase activity (9, 10). Moreover, SG can form in the absence of translation inhibition, indicating that SGs can form via multiple alternative pathways (11).

SGs contain a diverse proteome. In addition to stalled initiation complexes composed of translation initiation factors, SGs are comprised of many other RNA-binding proteins and non-RNA-binding proteins (12–15). Some hallmark SG RNA-binding proteins include T-cell intracellular antigen 1 (TIA-1), TIA-1-related protein (TIAR), and RasGAP-SH3-binding protein (G3BP) (16, 17). The SG proteome is enriched with proteins that contain intrinsically disordered regions (IDR), a motif that TIA-1, TIAR, and G3BP share, which is thought to be important in the assembly and maintenance of SGs by providing the multivalent interactions necessary for linking mRNP complexes (1, 18). Besides IDRs, SG assembly, maintenance, and disassembly can be modulated by a variety of ATP-dependent complexes and posttranslational modifications, including methylation, phosphorylation, and glycosylation (4, 13, 15, 17, 19). Some ATP-dependent complexes include the microtubule-dependent motors that transport mRNPs to SGs (20, 21) and mRNP or protein remodeling complexes (13, 22–25). There are more than 60 proteins that are associated with or have been reported to form foci and colocalize with hallmark SG markers under cellular stress (13, 15). Not all SGs are homogeneous; SGs can consist of a subset of proteins that are cell type specific and depend on the type and duration of an SG inducer (1, 26–28). SGs are highly dynamic structures. Fluorescence recovery after photobleaching (FRAP) experiments indicate most mRNAs and protein components can rapidly exchange in and out of SGs (16, 27–30), consistent with the notion that SGs have fluid-like properties. Weak multivalent interactions provided by IDRs contribute to the liquid-liquid phase separation properties of SGs and contribute to SG fusion, fission, and flow (1, 27, 31, 32).

It is now well established that many RNA and DNA viruses antagonize SG assembly and maintenance across species (33–35). However, the mechanisms by which SGs are inhibited are varied. Also, the significance of this inhibition and how it affects overall virus infection are not fully understood, since the consequences of inhibiting SGs are diverse. In poliovirus infection, SGs form initially, but at later times of infection through the action of the viral 3C protease, G3BP1 is cleaved, thereby inhibiting canonical SG formation to promote infection (36). Alternatively, some viruses indirectly affect SG formation. Alphaviruses and West Nile virus inhibit SG assembly by sequestering key SG components like TIA-1, TIAR, and G3BP to viral replication complexes (37–40). Recent studies have shown that the antiviral sensors RIG-I and PKR are activated upon binding to viral RNAs that are trapped in SGs, thereby triggering antiviral defense pathways and providing a possible basis for inhibition of SGs in many virus infections (41–43). Uncovering the links between SG and virus infection should provide insights into fundamental virus-host interactions.

Dicistroviruses are small, monopartite, positive-strand RNA viruses that primarily infect arthropods (44). Members include the *Cricket paralysis virus* (CrPV) and *Drosophila C virus* that can infect *Drosophila melanogaster*, which have provided excellent infection models to study fundamental virus-host interactions in insect cells. Other members include the honeybee viruses, *Israeli acute paralysis virus* and *Kashmir bee virus*, which have been linked to honey bee disease, and *Taura syndrome virus*, which has caused virus outbreaks in the shrimp industry (45–47). The RNA genome of dicistroviruses contains two main open reading frames (ORFs) encoding the viral nonstructural (ORF1) and structural proteins (ORF2). ORF1 and ORF2 are translated as a polyprotein, which is then processed by the viral 3C-like protease (44). Each ORF is driven by an independent internal ribosome entry site (IRES) that provides temporal and distinct regulation of viral protein expression (48, 49). Previous studies have revealed that dicistrovirus infection leads to modulation of a number of cellular processes that facilitate virus infection (50–59). CrPV and DCV infection of *Drosophila* cells lead to a rapid and dramatic shutoff of translation and transcription (48, 49, 60, 61). Despite inhibition of

host translation during infection, SG assembly is inhibited (62). Specifically, key SG protein markers such as Rox8 and Rasputin (Rin), *Drosophila* homologs of TIA1 and G3BP, respectively, do not aggregate. How dicistroviruses inhibit SG formation is not known.

Despite the limited number of viral proteins expressed from the dicistrovirus genome, it is probable that key viral proteins are modulating cellular processes to facilitate specific steps of the virus life cycle. For example, both CrPV and DCV encode 1A, a 168- and 99-amino-acid protein, respectively, that inhibits the antiviral RNA interference (RNAi) pathway (52, 53). Each protein functions in a different manner; DCV-1A is a double-stranded RNA (dsRNA) binding protein that sequesters viral dsRNA intermediates from the RNAi machinery, and CrPV-1A binds directly to and inhibits Ago2 activity. Ago2-deficient flies are hypersensitive to virus infection and succumb to death earlier than wild-type flies, highlighting the importance of this antiviral pathway in insect cells (53, 63). Currently, the viral proteins that modulate host translation, transcription, and SG assembly during dicistrovirus infection are not known.

Here, we discover that CrPV-1A modulates SG formation and inhibits host transcription. We also identify a key residue, R146, that is important for these functions of CrPV-1A and demonstrate that infection by mutant R146A CrPV in *Drosophila melanogaster* cells and adult fruit flies is attenuated. Our results indicate that besides inhibiting RNAi, CrPV-1A is a multifunctional protein that modulates several cellular functions to facilitate virus infection.

## RESULTS

CrPV infection modulates a number of cellular pathways, including host translation, transcriptional shutoff, and SG assembly (48, 49, 60, 62, 64). CrPV encodes at least 12 viral proteins, including 8 nonstructural and 4 structural proteins (61) (Fig. 1A). To identify viral proteins that mediate these processes, we subcloned each nonstructural and structural protein coding region into a *Drosophila* expression plasmid under the control of an actin (Act5C) promoter. We cotransfected two *Drosophila* expression plasmids into S2 cells, one plasmid that encodes firefly luciferase (Fluc) to monitor gene expression and a second plasmid that expresses the CrPV protein, and measured Fluc activity 2 days posttransfection (Fig. 1B). While the majority of CrPV proteins did not affect Fluc activity, CrPV-1A and 3C protease inhibited Fluc activity by >95% and >75%, respectively (Fig. 1B). Moreover, expression of 1A inhibited cell growth in S2 cells (Fig. 1C). For the remainder of the study, we focused on the role of CrPV-1A.

The loss of Fluc activity could be a result of CrPV-1A inhibiting overall translation and/or transcription. We first addressed whether CrPV-1A expression led to an inhibition of translation. Since expression of CrPV-1A affected cell viability, we used a transient expression approach by cotransfecting an *in vitro*-transcribed CrPV-1A RNA with a monocistronic Fluc RNA (mono-Fluc) and assayed for Fluc activity 10 h after transfection. CrPV-1A is fused in frame with a hemagglutinin (HA) tag for detection by immunoblotting, and all *in vitro*-transcribed RNAs are capped and contain a poly(A) tail. Surprisingly, transfection of CrPV-1A-HA RNA enhanced the expression of Fluc activity by 2-fold compared to transfection of a control RNA encoding DsRed (Fig. 1D). The stimulation of translation by CrPV-1A is unexpected, since CrPV infection in S2 cells results in a nearly complete inhibition of host translation (49, 60, 61). To address whether expression of CrPV-1A affected IRES translation, we transfected an *in vitro*-transcribed bicistronic CrPV minigenome RNA (Fig. 1E), which monitors both CrPV 5′ IRES (Renilla luciferase [Rluc])- and IGR IRES-mediated (Fluc) translation (48). Compared to the control DsRed-HA RNA transfection, 5′IRES-dependent Fluc activity increased approximately 2.5-fold in cells transfected with CrPV-1A-HA RNA, whereas IGR IRES-mediated Fluc activity was not affected (Fig. 1F). In summary, the translational stimulation of the reporter RNA by CrPV-1A is 5′-end dependent.

We next addressed whether CrPV-1A affected transcription (Fig. 2A). Here, instead of RNA, we cotransfected two *Drosophila* expression plasmids into S2 cells, one plasmid that encodes Fluc to monitor gene expression and a second plasmid that encodes

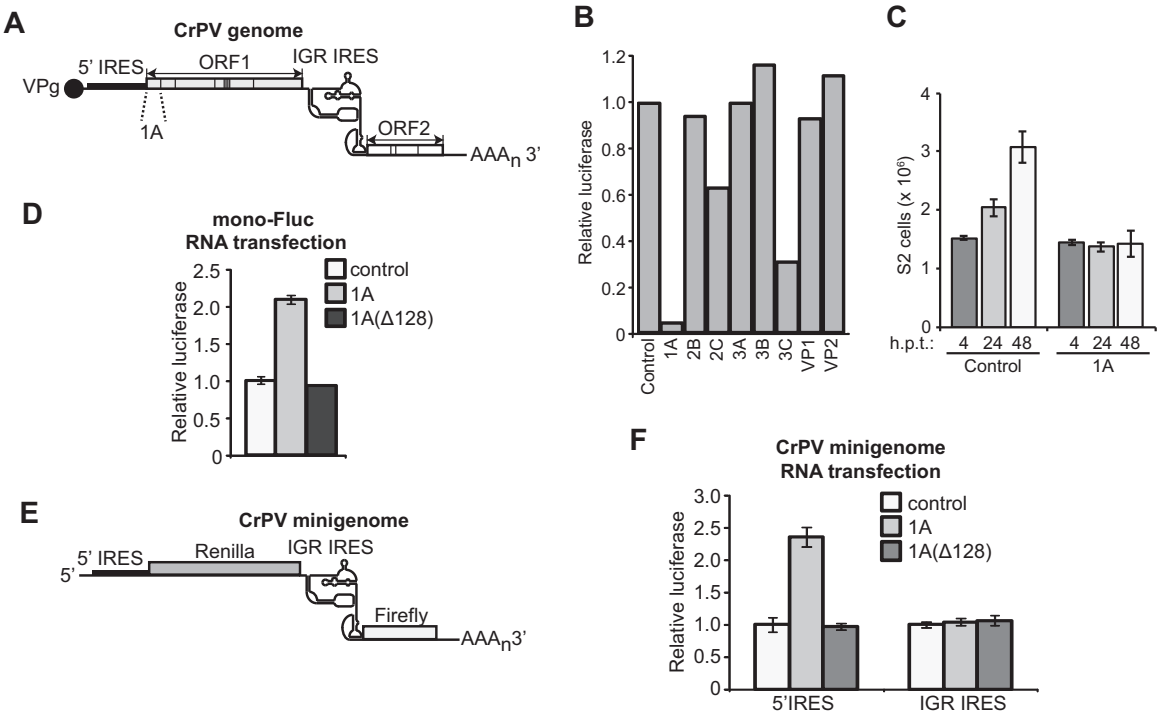


**FIG 1** CrPV-1A modulates gene expression. (A) Schematic of the cricket paralysis virus (CrPV) genome. (B) Luciferase activity from a *Drosophila* expression plasmid expressing Fluc cotransfected with the *Drosophila* expression plasmid expressing DsRed-HA (control) or the indicated HA-tagged CrPV viral protein. The expression plasmids are driven by the *Drosophila* Act5c promoter. (C) Total number of S2 cells after cotransfecting a *Drosophila* expression plasmid expressing CrPV-1A or DsRed (control) with a *Drosophila* expression plasmid expressing Fluc. S2 cells were counted at 4, 24, and 48 h posttransfection (h.p.t.). Luciferase activities from lysates of S2 cells were transfected with an *in vitro*-transcribed monocistronic Fluc mRNA (D) or the CrPV minigenome mRNA (E and F). Reporter mRNAs were cotransfected with *in vitro*-transcribed mRNA encoding DsRed-HA (control), 1A-HA (HA; hemagglutinin tag), or 1AΔ128-HA. Luciferase activity was measured 10 h posttransfection, and the results are normalized to control transfection (DsRed-HA). Shown are averages (± SD) from at least three independent experiments.

CrPV-1A-HA, and measured Fluc activities at 4, 24, and 48 h after transfection. At 24 h after transfection, there is a significant loss in Fluc activity (2-fold) when CrPV-1A-HA plasmid is cotransfected compared to the control DsRed-HA transfection (Fig. 2A). Northern blot analysis showed a decrease in steady-state mRNA levels of Fluc, supporting that CrPV-1A inhibits expression of Fluc at the transcriptional level (Fig. 2B).

Previous reports showed that the C-terminal 40 amino acids of CrPV-1A are important for suppressing RNAi (Fig. 2C) (52). Specifically, truncation of the last 40 amino acids of CrPV-1A(Δ128) abolishes CrPV-1A's ability to suppress RNAi. To determine whether this domain is important for CrPV-1A's ability to stimulate 5′-end-dependent translation, we compared cotransfection experiments using 1A and the truncation mutant CrPV-1A(Δ128) with the mono-Fluc and the CrPV minigenome reporter RNAs (Fig. 1D and F). Transfection of the mutant CrPV-1A(Δ128) did not affect 5′-end-dependent translation, suggesting that these effects on 5′-end-dependent translation are restricted to the last 40 amino acids of CrPV-1A (Fig. 1D and F). To precisely map which amino acids are important for this effect, we performed single alanine mutagenesis across residues 128 to 148 of CrPV-1A (Fig. 2C and D). We cotransfected the mutant CrPV-1A with the CrPV minigenome RNA and monitored 5′-untranslated region (UTR) IRES and IGR IRES translation. Out of the 18 mutations tested, only the R146A mutation was unable to stimulate 5′-end-dependent expression, which is similar to observations for CrPV-1A(Δ128) (Fig. 2D). Transfection of plasmids expressing wild-type CrPV-1A, but not CrPV-1A(Δ128) or CrPV-1A(R146A), resulted in decreased Fluc activity from an Fluc expression plasmid (Fig. 2A), suggesting that on top of inhibiting 5′-end-dependent translation, the last 40 amino acids and R146 of CrPV-1A also are important for inhibiting transcription. Expression of the wild type and mutants CrPV-1A(Δ128) and

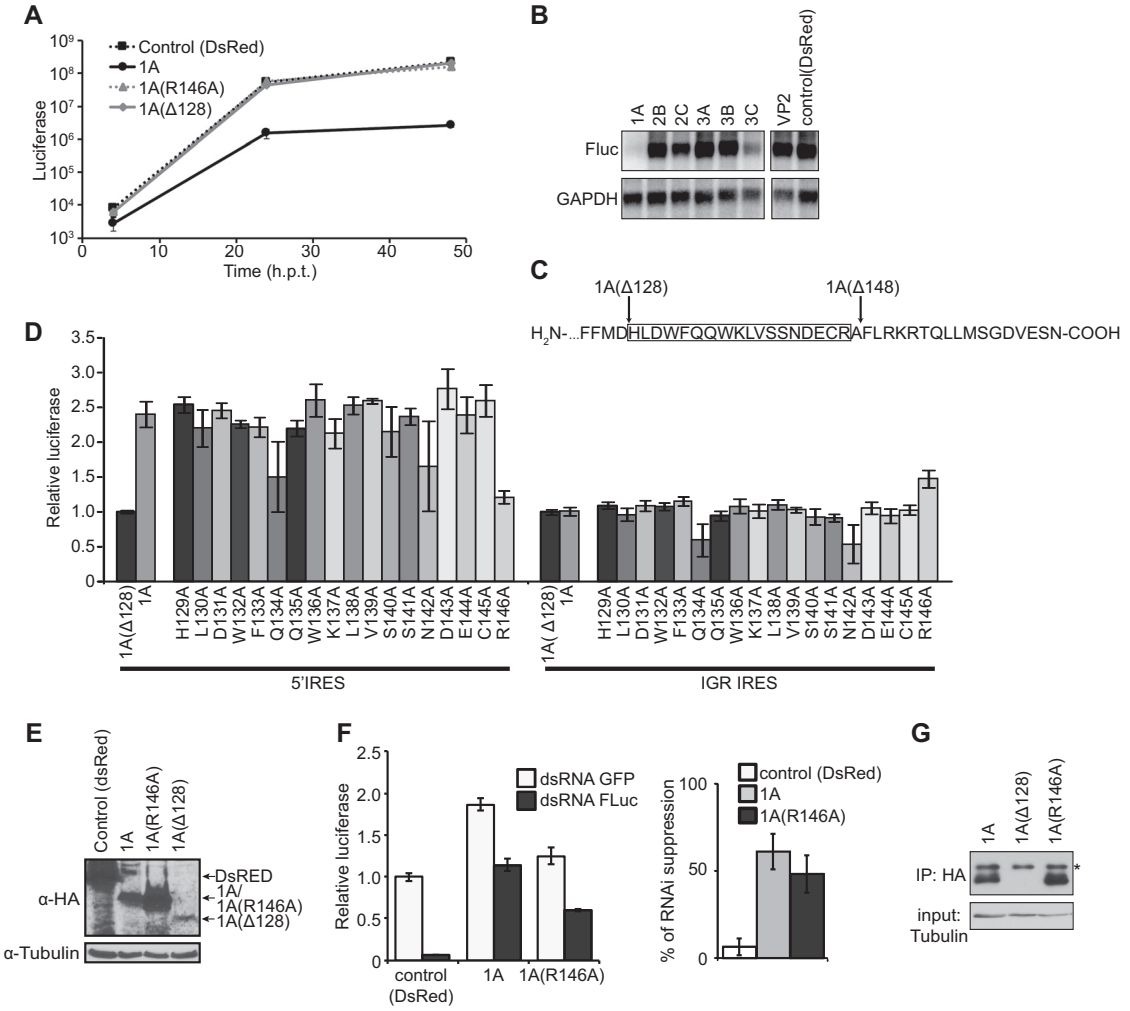


**FIG 2** Characterization of R146 of CrPV-1A. (A) Luciferase activity from a *Drosophila* expression plasmid expressing Fluc cotransfected with an expression plasmid expressing DsRed-HA (control), CrPV-1A-HA, CrPV-1A(R146A)-HA, or CrPV-1A(Δ128)-HA. The expression plasmids are driven by the *Drosophila* Act5c promoter. (B) Corresponding Fluc and glyceraldehyde-3-phosphate dehydrogenase (GAPDH) RNA levels as determined by Northern blotting shown in Fig. 1B. (C) Amino acid sequence of the C-terminal 40 amino acids of CrPV-1A. (D) Scanning alanine mutagenesis of CrPV-1A amino acid residues 128 to 146. Wild-type and mutant CrPV-1A mRNAs were cotransfected with the CrPV minigenome RNA reporter, and luciferase activities were measured 10 h posttransfection. Results are normalized to luciferase activities from cells expressing CrPV-1A(Δ128). (E) HA and tubulin antibody immunoblots of S2 cell lysates shown in panel A. (F) RNAi suppression activity in S2 cells. S2 cells were pretreated with dsRNA directed against Fluc (dsRNA Fluc) or GFP (dsRNA GFP) for 2 days, followed by cotransfection of an Fluc-containing reporter mRNA with DsRed (control), CrPV-1A-HA, or CrPV-1A(R146A)-HA mRNA. Four hours after transfection, Fluc activity was measured. All *in vitro*-transcribed mRNAs are capped and polyadenylated. (Left) Luciferase activities (*y* axis) are normalized to the cells pretreated with dsRNA GFP and transfected with DsRed (control) mRNAs. (Right) Percentage of RNAi suppression was normalized to Fluc activity of cells treated with dsRNA GFP. (G) HA immunoblotting of HA-immunoprecipitated (IP) lysates from S2 cells transfected with *in vitro*-transcribed CrPV-1A-HA or CrPV-1A(R146A)-HA RNA. As a loading control, the input lysates were immunoblotted for tubulin. Shown are averages (± SD) from at least three independent experiments.

CrPV-1A(R146A) was confirmed by immunoblot analysis, although CrPV-1A(Δ128) was expressed at much lower levels, which may reflect differences in protein stability (Fig. 2E).

Since CrPV-1A is reported to inhibit RNAi, we next asked whether CrPV-1A(R146A) can suppress this process (52). We pretreated S2 cells with double-stranded RNA (dsRNA) targeting Fluc or GFP RNA for 2 days, followed by transfection of the mono-Fluc RNA. As expected, pretreatment of cells with Fluc dsRNA suppressed Fluc activity by >90% compared to cells pretreated with GFP dsRNA (Fig. 2F). Cotransfection of CrPV-1A RNA inhibited RNAi-mediated suppression as reported previously (Fig. 2F) (52). Similarly, CrPV-1A(R146A) RNA also inhibited RNAi to the same extent as the CrPV-1A RNA (Fig. 2F). Expression of CrPV-1A and CrPV-1A(R146A) were confirmed by immuno-

precipitations with resin conjugated to HA antibody followed by immunoblotting with HA antibody (Fig. 2G). These results suggest that the stimulation of 5′-end-dependent translation and inhibition of transcription by CrPV-1A is independent of its ability to inhibit RNAi.

**CrPV R146 promotes virus infection.** We next investigated the effects of R146A on virus infection. Specifically, we introduced the R146A mutation into a previously generated CrPV infectious clone, CrPV-3 (65). Transfection of *in vitro*-transcribed CrPV-3(R146A) RNA in S2 cells resulted in virus production. We harvested virus and infected S2 cells with the wild type or CrPV-3(R146A) at an multiplicity of infection (MOI) of 10 and monitored protein synthesis by [$^{35}$S]Met/Cys pulse labeling, viral protein expression by immunoblotting, viral RNA by Northern blotting, and viral yields by a fluorescent focus-forming assay. Compared to wild-type infection, CrPV-3(R146A) infection delayed overall inhibition of host translation and decreased viral protein synthesis at the earlier times of infection (Fig. 3A to C). In agreement, immunoblot analysis showed that CrPV-1A, RNA-dependent RNA polymerase (RdRp), and VP2 structural protein levels are decreased in CrPV-3(R146A)-infected compared to CrPV-3-infected cells (Fig. 3D). CrPV genomic RNA levels were also lower in CrPV-3(R146A) infection than in wild-type infection (Fig. 3E). Finally, intracellular and extracellular viral yields were reproducibly lower in CrPV-3(R146A)-infected S2 cells than in CrPV-3-infected cells at an MOI of 0.1 at 6 and 12 h postinfection (h.p.i.) (Fig. 3F). These results demonstrate that residue R146 is required for productive CrPV infection in S2 cells.

To further examine the effects of CrPV-1A(R146A) on virus replication and translation, we introduced R146A into a CrPV2(Fluc) replicon, which replaces the ORF2 structural protein with the Fluc gene under the control of the IGR IRES (Fig. 3G) (48). The replicon provides a direct readout of viral translation and replication. As previously shown, transfection of the CrPV-2(Fluc) RNA resulted in an increase in Fluc activity after 12 h posttransfection, indicative of replication (Fig. 3H). In contrast, the introduction of a stop codon in ORF1 [CrPV-2(Fluc)-ORF1$^{stop}$], which blocks expression of all nonstructural proteins, or the R146A mutation resulted in dampened Fluc activity (Fig. 3H). These results support the conclusion that residue R146 of CrPV-1A is essential for CrPV replication in S2 cells.

**R146 residue in the CrPV-1A protein is essential for transcriptional inhibition during virus infection.** Our results suggest that CrPV-1A is important for inhibiting transcription of an expression plasmid (Fig. 2A). To assess whether host transcription is affected, we monitored transcription of endogenous genes in wild-type- and CrPV-3(R146A)-infected S2 cells. Specifically, we used a 4-thiouridine (4sU) approach whereby 4sU pulse labeling of newly synthesized RNAs can be captured through biotinylation of the thio group followed by purification using streptavidin bead pulldown (66, 67). Purified 4sU-labeled mRNAs were monitored by real-time reverse transcription-PCR (RT-PCR) (Fig. 4A). We infected S2 cells with the wild type or mutant CrPV-3(R146A) and pulse labeled them with 4sU for 2, 4, or 6 h (Fig. 4A). After extracting total RNA, thio groups were biotinylated using MTS-biotin (Fig. 4A) (67). Streptavidin-horseradish peroxidase (Strep-HRP) immunoblotting readily detected the 18S/28S rRNA in mock-infected cells (Fig. 4B). In contrast, CrPV infection leads to loss of rRNA detection by Strep-HRP, consistent with previous reports that overall rRNA transcription is inhibited during CrPV infection (Fig. 4B) (48). On the other hand, CrPV-3(R146A)-infected cells only lead to a modest loss of rRNA transcription. To determine whether RNA polymerase II (Pol II)-mediated mRNA synthesis was affected, we monitored two housekeeping genes, Act5C and Rpl13, from purified 4sU-labeled RNA. Whereas CrPV-3 infection led to a dramatic shutoff of transcription compared to mock infection, CrPV-3(R146A) infection did not affect Act5C and Rpl13 transcription (Fig. 4C). These results further demonstrate that R146 is important for CrPV-1A to inhibit transcription during CrPV infection.

**CrPV-1A inhibits stress granule formation.** Our results suggest that in addition to inhibiting RNAi, CrPV-1A can also perturb host transcription and stimulate 5′-end-

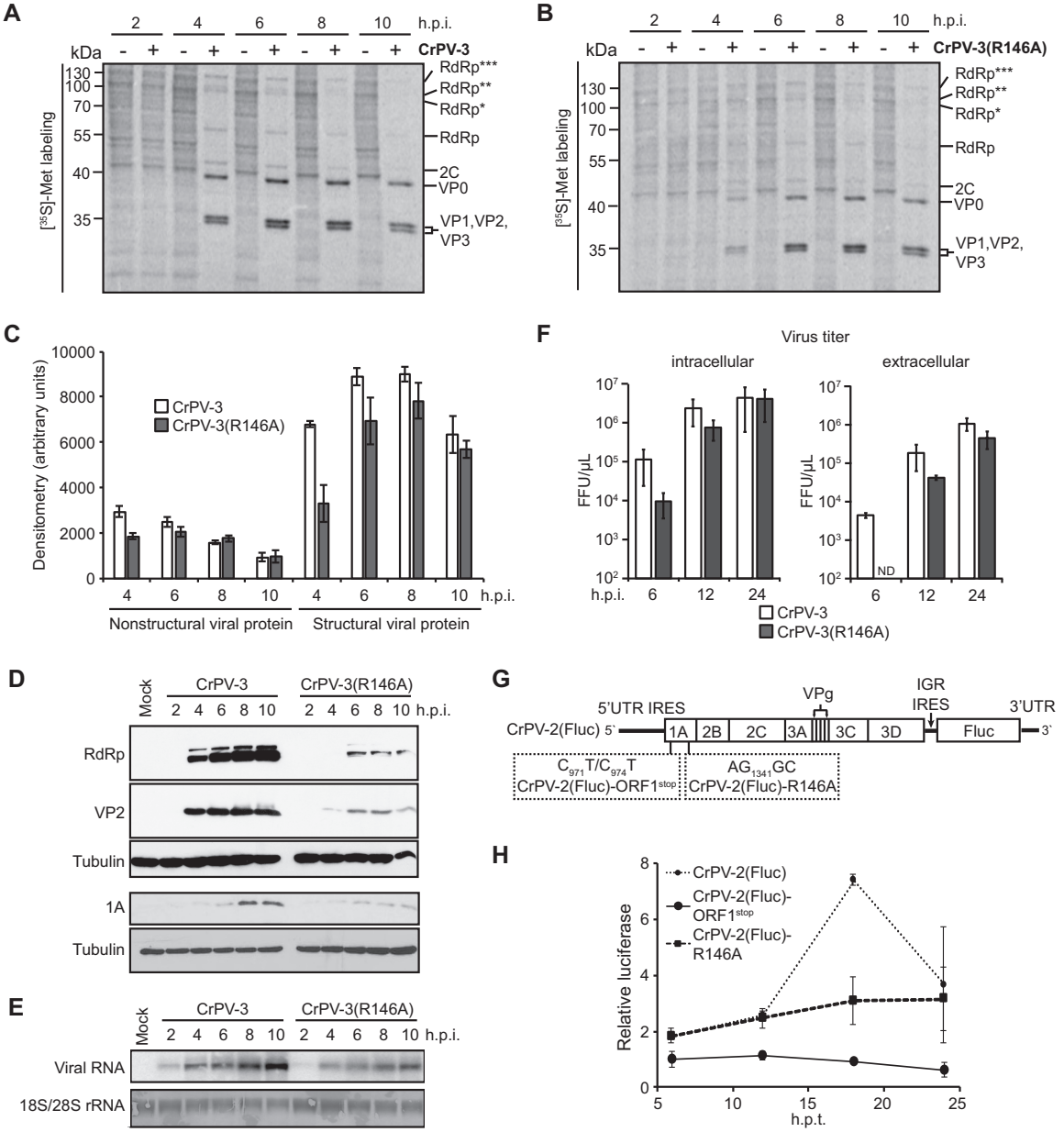


**FIG 3** CrPV-3(R146A) infection is attenuated in *Drosophila* S2 cells. Autoradiography of [$^{35}$S]Met/Cys pulse-labeled protein lysates from S2 cells infected with CrPV-3 (A) or CrPV-3(R146A) (B) at an MOI of 10 resolved on a 12% SDS-PAGE gel. Cells were metabolically labeled with [$^{35}$S]Met/Cys for 30 min at the end of each time point (h.p.i.). (C) Raw densitometric quantitation of [$^{35}$S]Met/Cys pulse-labeled viral nonstructural (RdRp***, RdRp**, RdRp*, RdRp, and 2C) and structural proteins (VP0, VP1, VP2, and VP3) during CrPV-3 or CrPV-3(R146A) infection from three independent experiments (± SD). RdRp*, RdRp**, and RdRp*** denote polyproteins containing RdRp. (D) Immunoblots of lysates collected from mock-, CrPV-3-, and CrPV-3(R146A)-infected S2 cells (MOI of 10). (E) Viral RNA levels in cells infected with CrPV-3 or CrPV-3(R146A) at an MOI of 10 were detected by Northern blotting. Methylene blue staining of the blot is shown below. (F) Viral titers from intracellular and extracellular virus from CrPV-3- or CrPV-3(R146A)-infected cells at 6, 12, and 24 h p.i. (MOI of 0.1). Titers were calculated as FFU (FFU/$\mu$l ± SD) from three independent experiments. (G) Schematics of the CrPV-2(Fluc), CrPV-2(Fluc)-ORF1$^{stop}$, and CrPV-2(Fluc)-R146A replicons. (H) Fluc activities from cells transfected with CrPV-2(Fluc), CrPV-2(Fluc)-ORF1$^{stop}$, and CrPV-2(Fluc)-R146A replicons at 6, 12, 18, and 24 h posttransfection (h.p.t.). The results are normalized to the Fluc activity at 6 h.p.t. from cells transfected with CrPV-2(Fluc)-ORF1$^{stop}$. Shown are averages (± SD) from at least three independent experiments.

dependent translation of reporter RNAs (Fig. 1 and 2). Given the effects of CrPV-1A on host gene expression, we next examined whether CrPV-1A had an effect on SG assembly, as it is known that CrPV inhibits SG formation during infection (62). We generated a stable S2 cell line expressing a green fluorescent protein (GFP)-Rasputin fusion protein (RinGFP). Rin is the *Drosophila* homolog of human G3BP and is a hallmark SG marker (68). Treatment of the stable cell line with the eIF4A helicase modulator PatA

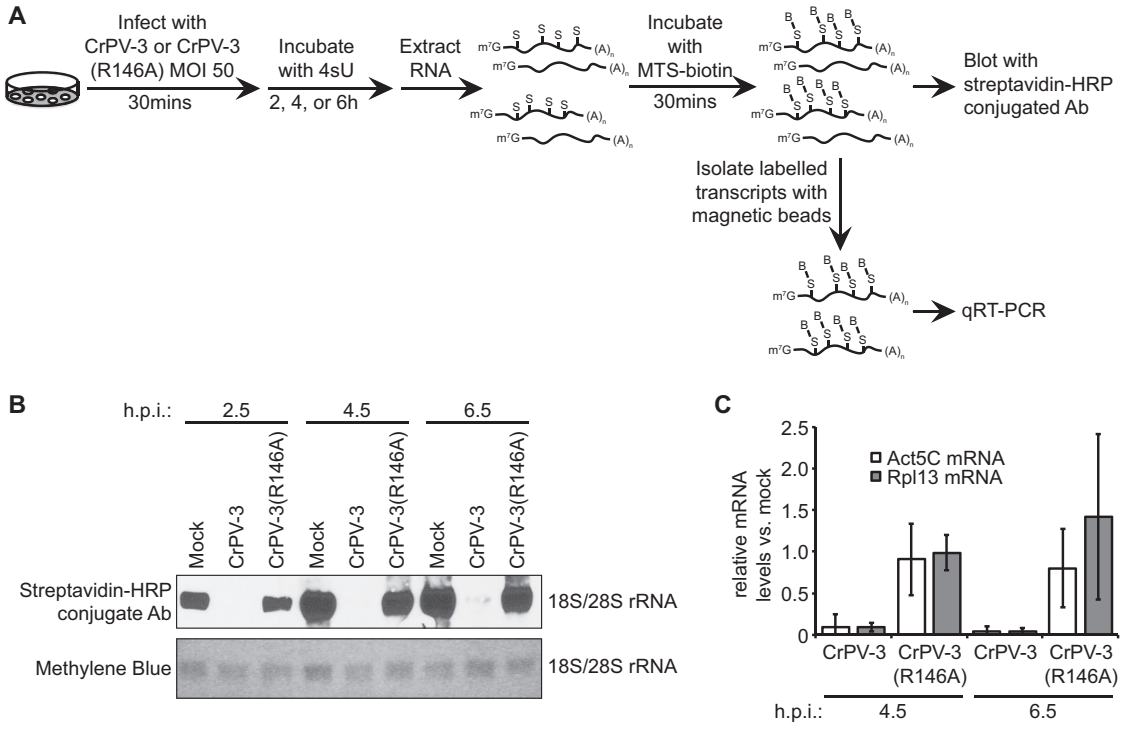


**FIG 4** R146 residue is important for transcriptional repression during CrPV infection in S2 cells. (A) Scheme of metabolic mRNA labeling in mock-, CrPV-3-, or CrPV-3(R146A)-infected S2 cells. Mock-, CrPV-3-, or CrPV-3(R146A)-infected S2 cells (MOI of 50) (adsorbed for 30 min) were labeled with 200 $\mu$M 4-thiouridine (4sU) for 2, 4, or 6 h. Subsequently, total RNA was extracted and biotinylated with 5 $\mu$g MTS-biotin for 30 min. (B) 4sU-labeled 28S rRNA was detected upon blotting with Streptavidin-HRP-conjugated antibody (Ab). Methylene blue staining of the blot is shown below. (C) Quantitative reverse transcription-PCR (qRT-PCR) of newly transcribed, purified 4sU-labeled actin and Rpl13 mRNAs from S2 cells infected with CrPV-3 or CrPV-3(R146A). The results are individually normalized to mock infection. Shown are averages ($\pm$ SD) from at least three independent experiments.

(69) resulted in visible RinGFP foci, indicative of SG formation (Fig. 5A, green fluorescence). As shown in the box plot (Fig. 5B), the number of visible RinGFP foci per cell increased upon PatA treatment. Cells transfected with CrPV 1A RNA followed by PatA treatment are resistant to RinGFP focus formation, whereas cells transfected with CrPV-1A(R146A) are not (Fig. 5A). Quantitation of the number of visible RinGFP foci in cells expressing CrPV-1A-HA or CrPV-1A(R146A)-HA is shown in the box plot (Fig. 5B). The median number of RinGFP foci induced by PatA is approximately 4 foci in cells expressing CrPV-1A(R146A) compared to a median of 0 foci in cells expressing CrPV-1A (Fig. 5B). By immunoblotting, RinGFP levels are unchanged in S2 cells transfected with CrPV-1A-HA or CrPV-1A(R146A)-HA; thus, inhibition of RinGFP focus assembly by CrPV-1A is not due to loss of RinGFP (Fig. 5C). Interestingly, HA-tagged CrPV-1A is primarily localized in the nucleus (Fig. 5A, red fluorescence). In summary, these results demonstrate that CrPV-1A can inhibit PatA-induced RinGFP focus assembly.

We next examined the effects of CrPV-1A on SG assembly during CrPV infection. We infected S2 cells stably expressing RinGFP with wild-type CrPV-3 or CrPV-3(R146A) at an MOI of 50 (Fig. 6A). We monitored RinGFP focus formation and poly(A) mRNA using oligo(dT)-Cy5 fluorescent *in situ* hybridization (FISH). As shown previously, even though overall host translation is inhibited (62), only 13% of $\geq$3 RinGFP foci per cell were observed in CrPV-infected S2 cells, similar to that observed in mock-infected cells, indicating that SG assembly is not induced (Fig. 6A). In contrast, in CrPV-3(R146A)-infected cells, the number of RinGFP foci steadily increases at 4 h p.i. and 8 h p.i., with at least 41% of cells showing $\geq$3 RinGFP foci per cell. Furthermore, the median number of RinGFP foci increases during CrPV-3(R146A) infection but not in wild-type infection (Fig. 6B). As shown previously (62), RinGFP protein levels were unaltered in CrPV-3- and CrPV-3(R146A)-infected S2 cells, indicating that the loss of RinGFP foci in CrPV-infected cells is not due to loss of RinGFP protein (Fig. 6C).

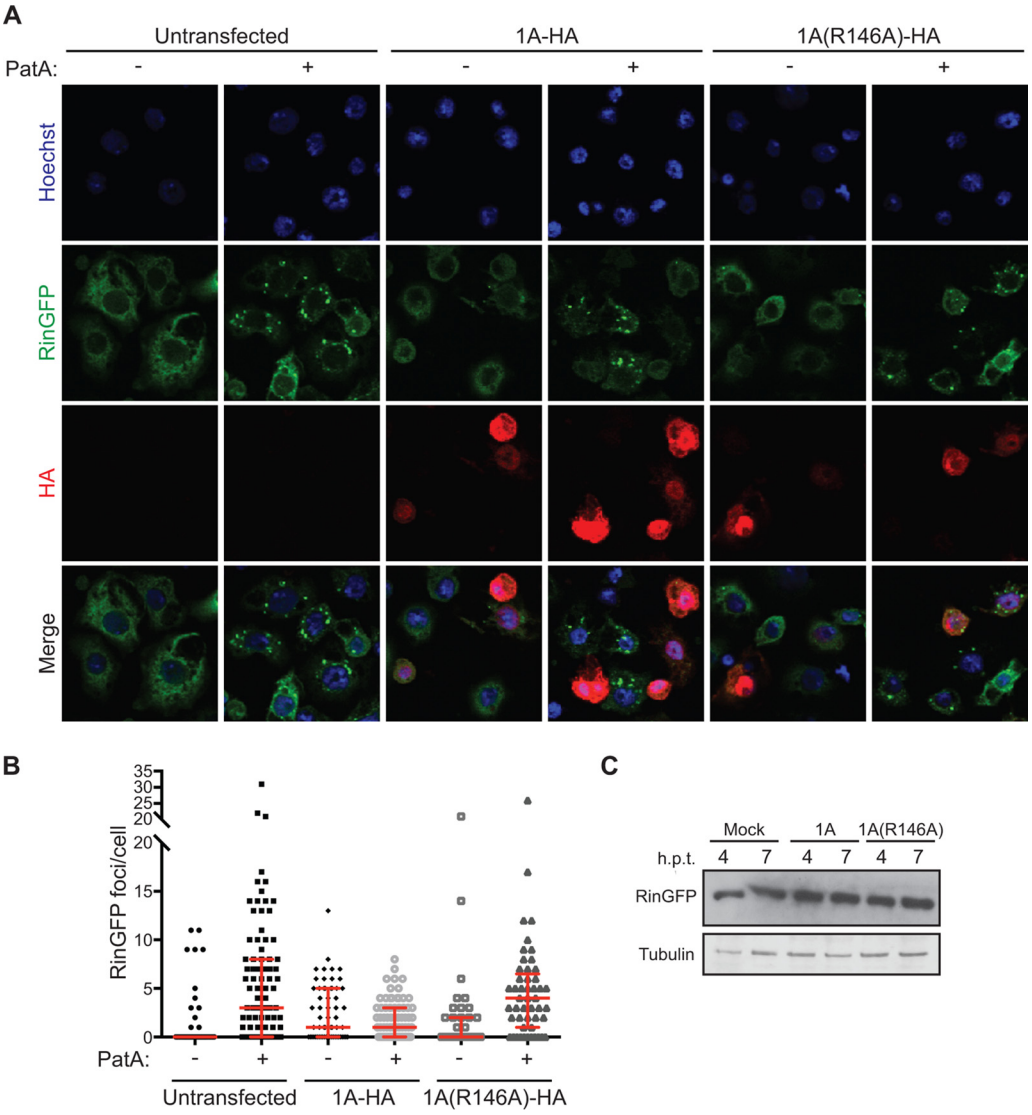


**FIG 5** CrPV-1A inhibits PatA-induced SG assembly. (A) S2 cells stably expressing a fusion RinGFP protein (green fluorescence) were transiently transfected with RNAs encoding CrPV-1A-HA or CrPV-1A(R146A)-HA for 9 h and then treated with DMSO or 50 nM pateamine A (PatA) for 1 h. S2 cells expressing CrPV-1A-HA or CrPV-1A(R146A)-HA are shown as red fluorescence. Nuclei were stained with Hoechst dye (blue fluorescence). (B) Box plot of the number of RinGFP foci per cell with medians and quartiles indicated by horizontal lines. At least 50 cells were counted for each condition from two independent experiments. (C) GFP and tubulin antibody immunoblots of S2 cell lysates expressing 1A-HA or 1A(R146A)-HA for the indicated times posttransfection.

In contrast to RinGFP, poly(A) foci are readily formed in both wild-type- and CrPV-3(R146A)-infected cells (Fig. 6D). Consistent with our previous findings (62), there was no or very little overlap between poly(A) foci and RinGFP foci in CrPV-3-infected cells. However, a subset of poly(A) foci overlapped with RinGFP foci in CrPV-3(R146A)-infected cells. To address whether the poly(A) foci are viral RNAs, we monitored CrPV replication intermediates using a dsRNA antibody (62, 70). In both CrPV-3- and CrPV-3(R146A)-infected cells, dsRNA staining increased over time but did not overlap RinGFP (Fig. 6E). These results suggest that R146 is important for CrPV-1A to inhibit SG formation.

To further examine the effects of CrPV-1A, we challenged CrPV-3 and CrPV-3(R146A) infection with PatA for 1 h to induce SGs (Fig. 7A). As previously reported (62), PatA treatment of mock-infected cells resulted in an increase in SG formation (58% of the cells having $\geq$3 RinGFP foci) and a median of 3 foci per cell (Fig. 7B). In contrast, PatA treatment of CrPV-infected cells at 4, 6, and 8 h p.i. resulted in reduced numbers of cells

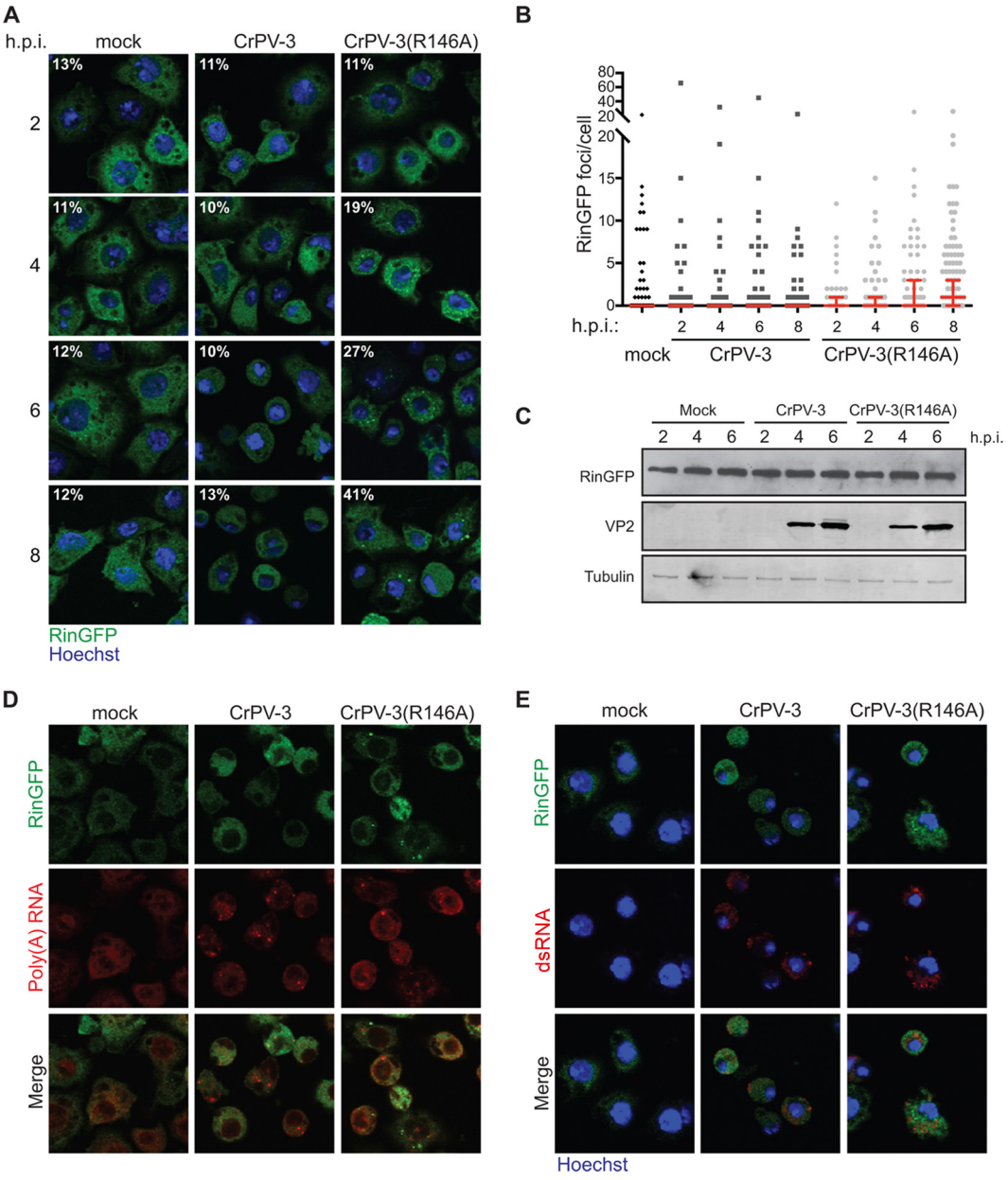


**FIG 6** CrPV-1A modulates SG assembly during virus infection. (A) Stable RinGFP S2 cells were mock infected or infected for 2, 4, 6, or 8 h with CrPV-3 or CrPV-3(R146A) virus at an MOI of 50. Cells were fixed and stained with Hoechst (blue fluorescence). Percentages indicate the proportion of cells with three or more visible RinGFP foci. (B) Box plot of the number of RinGFP foci in individual cells with medians and quartiles indicated by horizontal lines. At least 50 cells were counted for each sample from two independent experiments. (C) GFP, VP2, and tubulin antibody immunoblots of S2 cell lysates infected with CrPV-3 or CrPV-3(R146A) at an MOI of 10 for 2, 4, and 6 h p.i. Poly(A) RNA and viral RNA were monitored by FISH (red fluorescence) (D) or by dsRNA antibody (red fluorescence) staining (E), respectively. Shown are representative images from two independent experiments.

with RinGFP foci, indicating that CrPV infection prevents PatA-induced SG assembly. In CrPV-3(R146A)-infected cells, PatA treatment increased the number of RinGFP foci at all time points (Fig. 7A and B), further supporting that R146 is essential for inhibition of SGs during CrPV infection.

**Stress granule assembly during CrPV-3(R146A) infection in S2 cells is sensitive to inhibition of transcription.** Given that CrPV-1A may inhibit host transcription (Fig. 2), we next asked whether there is a link between host transcription and SG formation. To address this, we incubated S2 cells with actinomycin D (ActD) to inhibit all three RNA polymerase activities and then challenged them with PatA treatment to induce RinGFP

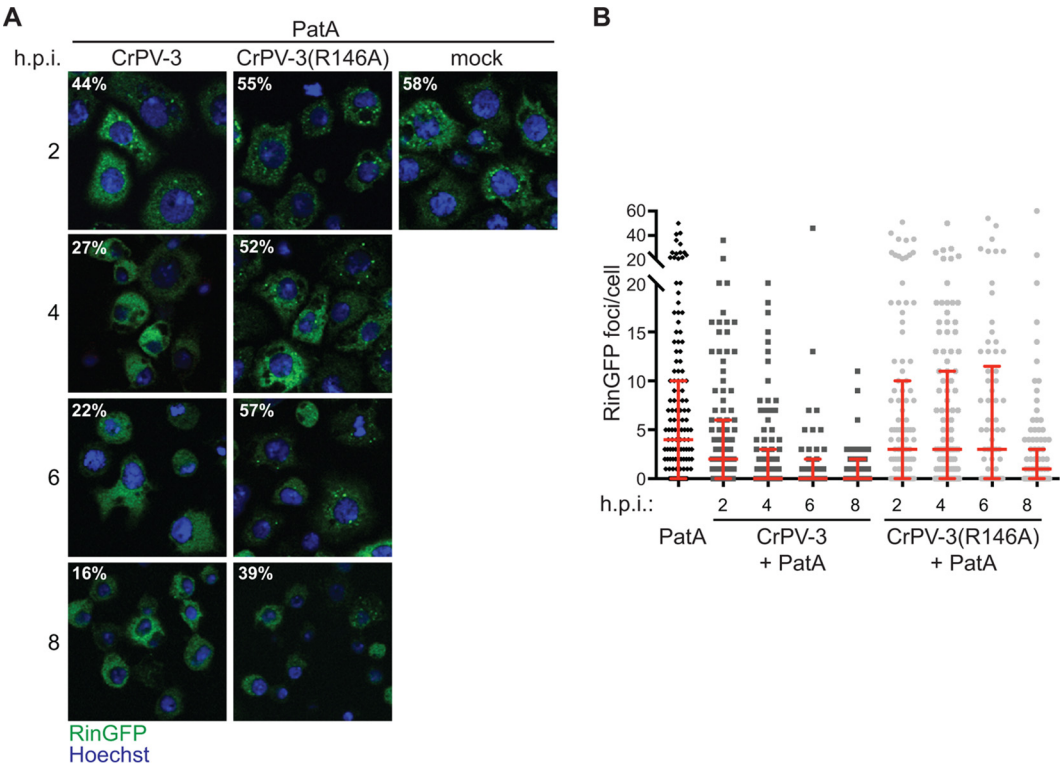


**FIG 7** Pateamine A treatment induces stress granules in CrPV-3(R146A)-infected S2 cells. (A) Infected cells were treated with 50 nM PatA to induce SGs for 1 h before the indicated time postinfection. (B) Box plot of the number of RinGFP foci in individual cells, with medians and quartiles indicated by horizontal lines. At least 50 cells were counted for each sample from two independent experiments.

foci (Fig. 8A). Compared to PatA treatment, which increases the number of RinGFP foci per cell, actinomycin D (ActD)-treated cells were resistant to PatA treatment, leading to a reduced number of RinGFP foci, suggesting that inhibition of transcription can influence RinGFP SG formation (Fig. 8A and B).

To determine whether inhibiting transcription affects SG in infected cells, we treated CrPV-3- or CrPV-3(R146A)-infected S2 cells with ActD at 2 h p.i. and examined RinGFP focus formation at 8 h p.i. (Fig. 8C and D). With or without ActD treatment, CrPV-3-infected cells showed relatively low percentages of cells with ≥3 RinGFP foci and a relatively low median number of RinGFP foci per cell, similar to that observed in mock-infected cells (Fig. 8C and D). As shown previously (Fig. 6A), in CrPV-3(R146A)-infected S2 cells, 39% of cells showed ≥3 RinGFP foci and an increase in the median number of RinGFP foci per cell. In contrast, only 6% of CrPV-3(R146A)-infected S2 cells showed ≥3 RinGFP foci when ActD was added and a low median number of RinGFP foci per cell (Fig. 8C and D). These results demonstrate that shutoff of transcription by ActD treatment can inhibit SG assembly during CrPV-3(R146A) infection and indicates that shutoff of host transcription by CrPV-1A likely contributes to inhibition of SG assembly during infection.

Since the R146A mutation lowers virus fitness (Fig. 3F) and abolishes CrPV-1A's function to inhibit transcription (Fig. 4), we asked if CrPV-3(R146A) virus infectivity is restored when transcription is shut off by ActD treatment. S2 cells were pretreated with ActD for 1 h, followed by CrPV-3 or CrPV-3(R146A) infection at an MOI of 0.1 for 6 h. Cells were harvested and viral yield quantitated. As shown previously (Fig. 3F), viral yield was significantly less in CrPV-3(R146A)-infected cells than in CrPV-3-infected cells ($P < 0.016$). In contrast, pretreating S2 cells with ActD for 1 h increased viral yield significantly in both CrPV-3-infected (~3-fold; $P < 7.1 \times 10^{-4}$) and CrPV-3(R146A)-infected (~20-fold; $P < 7.1 \times 10^{-5}$) cells (Fig. 8E). Moreover, viral yield was similar between wild-type and mutant virus infection in ActD-pretreated cells (Fig. 8E). These

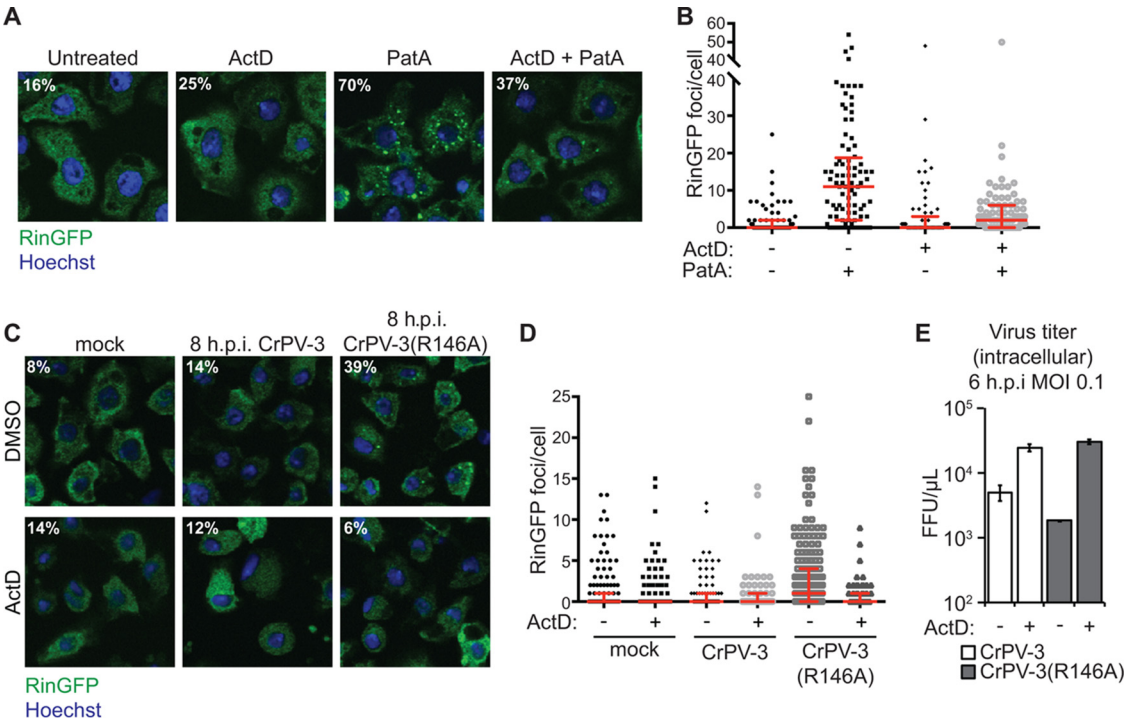


**FIG 8** Addition of actinomycin D during CrPV-3(R146A) infection inhibits SG assembly. (A) S2 cells stably expressing RinGFP (green fluorescence) pretreated with 5 $\mu$g/$\mu$l ActD or DMSO for 1 h were incubated with 50 nM PatA for 1 h to induce SGs. Cells were fixed and stained with Hoechst (blue fluorescence). Percentages indicate the proportion of cells with at least three or more visible RinGFP foci. (B and D) Box plot of the number of RinGFP foci in individual cells, with medians and quartiles indicated by horizontal lines. At least 50 cells were counted for each sample. (C) CrPV-3- or CrPV-3(R146A)-infected S2 cells (MOI of 50) stably expressing RinGFP (green fluorescence), a marker of SGs, were treated with DMSO or 5 $\mu$g/$\mu$l actinomycin D (ActD) 2 h postinfection. RinGFP foci were monitored at 8 h p.i. Genomic DNA was stained with Hoechst (blue fluorescence). Percentages indicate the proportion of cells with at least three RinGFP foci. (E) Viral titers (intracellular) from CrPV-3- or CrPV-3(R146A)-infected cells pretreated with 5 $\mu$g/$\mu$l ActD for 1 h at 6 h.p.i. (MOI of 0.1). Titers were calculated as FFU (FFU/$\mu$l $\pm$ SD) from three independent experiments.

results demonstrate that inhibition of transcription by CrPV-1A is key for inhibiting SG formation in CrPV infection and facilitates productive CrPV infection in S2 cells.

**CrPV-3(R146A) infection in *Drosophila melanogaster* is attenuated.** Given that CrPV-3(R146A) is less productive than CrPV-3 virus in S2 cells (Fig. 3F), we next asked whether this residue is important for infection in a more physiological context using an injection model in adult *Drosophila* flies. A total of 5,000 fluorescent focus-forming units (FFU) of CrPV-3, CrPV-3(R146A), or phosphate-buffered saline (PBS) was injected intrathoracically in *Drosophila melanogaster* (*iso-w1118*). Wild-type CrPV-3 injection led to death by 4 to 5 days postinjection (Fig. 9) (65), whereas PBS injection resulted in minimal mortality. In contrast, injection of CrPV-3(R146A) led to a delay of mortality compared to wild-type virus, with only 50% of the animals succumbing to death by 10 to 12 days after injection (Fig. 9). These results demonstrate that residue R146 of CrPV-1A is critical for productive infection not only in cells but also in adult fruit flies.

**CrPV-1A can inhibit stress granule assembly in HeLa cells.** SG formation is a conserved process in response to environmental cellular stress observed in many eukaryotes (71). Given that CrPV-1A can inhibit SG assembly in *Drosophila* S2 cells, we investigated whether CrPV-1A expression can affect SG assembly in HeLa cells. As previously reported (9, 10), PatA treatment of HeLa cells resulted in robust focus formation containing poly(A) RNA and G3BP1, indicative of SG formation (Fig. 10A and C). In contrast, transfection of a mammalian plasmid expressing CrPV-1A but not CrPV-1A(R146A) in HeLa cells challenged with PatA led to diffuse poly(A) RNA and G3BP1 staining (Fig. 10A and C). In support of this finding, the number of G3BP foci per cell was quantified; G3BP foci in untransfected cells or cells expressing CrPV-1A(R146A) increase dramatically upon PatA treatment, whereas cells expressing CrPV-1A do not

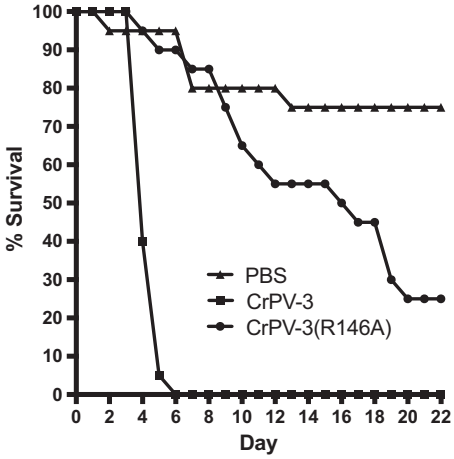


**FIG 9** Infection of CrPV-3(R146A) is attenuated in adult flies. Depicted is the survival of isogenic $w^{1118}$ flies (10 males and 10 females) that were injected intrathoracically with 5,000 FFU of CrPV-3, CrPV-3(R146A), or PBS. Mortality was monitored daily. Shown is a representative graph from two independent experiments.

(Fig. 10B). Immunoblot analysis confirmed expression of both proteins (Fig. 10D). These results suggest that CrPV-1A can disrupt SG formation via a conserved mechanism in insect and human cells.

## DISCUSSION

Viruses of many classes can modulate SG formation and impact virus infections (33, 34). The mechanisms that underlie this process and the effects that it has on the host to facilitate infection are not fully understood. Using the dicistrovirus CrPV as a model, we have identified a virus-encoded protein, 1A, that inhibits SG formation in CrPV-infected *Drosophila* S2 cells and human HeLa cells. Furthermore, using a 4sU labeling approach, we showed that CrPV-1A also inhibits host transcription, similar to that observed during CrPV infection in *Drosophila* cells. We propose that the shutoff of host transcription by CrPV-1A indirectly modulates SG assembly. Our data also indicate that these effects by CrPV-1A are independent of its property of suppressing the antiviral RNAi response (Fig. 2F), suggesting that CrPV-1A is multifunctional. We identified a key R146 residue that is important for mediating these effects and showed that introducing mutation R146A in the CrPV-3 infectious clone attenuates virus infection in S2 cells and adult fruit flies. Importantly, challenging CrPV-3(R146A)-infected cells with ActD, which mimics transcriptional shutoff, decreases SG formation and increases viral yield, consistent with the model that transcription shutoff by CrPV-1A promotes CrPV infection. Our data indicate that CrPV-1A has multiple functions affecting cellular processes to promote infection.

Our results indicate that CrPV-1A is nuclear localized and inhibits Pol III-mediated rRNA transcription (Fig. 4 and 5). We also showed that CrPV-1A inhibits transcription of a subset of mRNAs (Fig. 4C). Given that transcription is not repressed in CrPV-3(R146A)-infected cells, we propose that CrPV-1A is responsible for host transcriptional shutoff during infection, which is consistent with recent reports that dicistrovirus infection results in inhibition of transcription (48, 64). A large body of research suggests that inhibition of transcription is beneficial for viruses (72–74). Typically, this strategy is employed by viruses to inhibit antiviral responses triggered upon infection. In *Drosophila*, several immune pathways, such as the IMD and TOLL pathways, are activated in response to pathogens (75, 76). It is likely that transcriptional shutoff by CrPV-1A dampens transcription of innate immune genes in order for CrPV to evade antiviral responses and allow viral replication. Transcriptome analyses during dicistrovirus infection in S2 cells and *Drosophila melanogaster* reveal steady-state mRNA level changes that may relate to transcriptional regulation (50, 51, 57, 58, 64, 77). Whether or not host

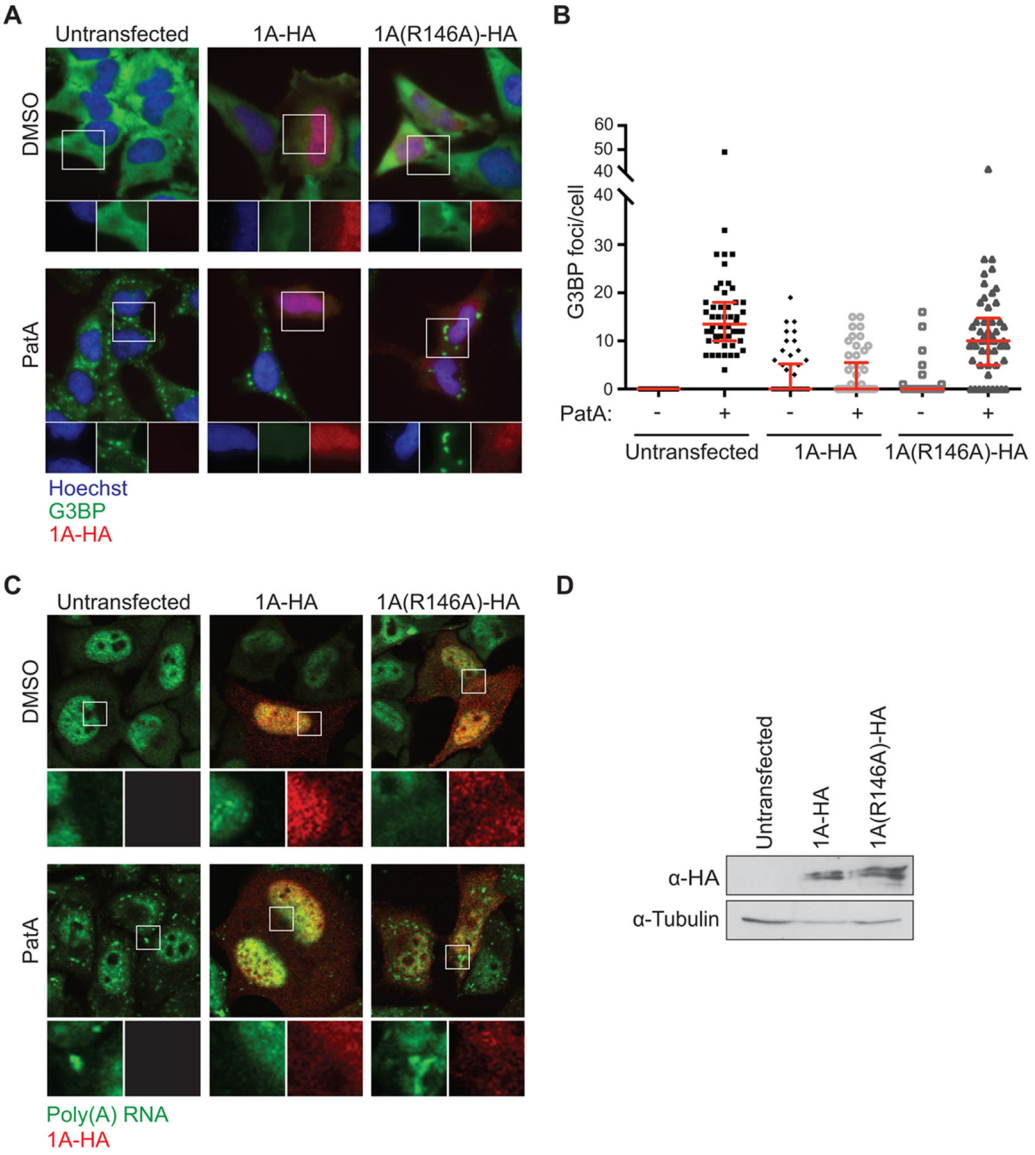


**FIG 10** CrPV-1A inhibits SG assembly in response to PatA treatment in HeLa cells. HeLa cells transiently transfected with mammalian expression plasmids encoding CrPV-1A-HA or CrPV-1A(R146A)-HA were treated with 50 nM PatA for 1 h. (A) HeLa cells were immunostained with $\alpha$-HA antibody (red fluorescence) and G3BP antibody (green fluorescence), a marker of SGs. (B) Box plot of the number of G3BP foci per cell, with the medians and quartiles indicated by horizontal lines. At least 50 cells were counted for each condition from three independent experiments. (C) HeLa cells were immunostained with $\alpha$-HA antibody (red fluorescence), and poly(A) RNA, a marker of SGs, was detected by *in situ* hybridization using Cy5-oligo(dT) (green fluorescence) (40). (D) Western blot analysis of CrPV-1A-HA and CrPV-1A(R146A)-HA using $\alpha$-HA and $\alpha$-tubulin antibodies.

transcription is inhibited in its entirety, perhaps using a more precise 4sU pulse-labeling approach, and how CrPV-1A accomplishes this mechanistically warrant further investigation.

Several lines of evidence indicate that transcriptional shutoff via CrPV-1A affects SG assembly in infected cells. (i) Infection with CrPV-3(R146A) results in increased RinGFP foci, which is correlated with loss of transcriptional repression in CrPV-3-infected cells. (ii) Expression of the wild type but not mutant CrPV-3(R146A) inhibits SG formation. (iii) ActD addition to S2 cells limits PatA-induced SG assembly. (iv) ActD addition to CrPV-3(R146A)-infected cells reduces SG assembly similar to that observed in wild-type infection and restores viral yield. Since mRNAs are thought to provide the multivalent interactions necessary for forming SGs (1), it is possible that transcriptional repression limits the overall pool of cytoplasmic mRNAs and thereby reduces the number of

mRNAs aggregating in SG foci. However, we have shown that poly(A) mRNAs still assemble during CrPV infection (62), suggesting that a pool of nontranslating mRNAs exists in infected cells, and the effects of SG inhibition may be due to loss of newly synthesized transcripts. A number of studies have demonstrated that limiting the cytoplasmic mRNA pool can inhibit SG formation. For example, trapping mRNAs on polysomes by blocking translation elongation can decrease SG assembly (16). In addition, *in vitro* SG and RNP granule assembly studies demonstrate that RNA facilitates granule formation (31, 78, 79). Furthermore, the influenza nonstructural protein PA-X depletes cytoplasmic mRNAs and limits SG assembly (80). In poliovirus infection, assembly of noncanonical SGs consisting of TIA-1 is sensitive to ActD treatment (81). However, another report has shown that inhibiting transcription by ActD does not affect SG assembly (28). The discrepancy in our findings is not clear but may be due to the duration of ActD treatment and cell type specificities.

The benefits of inhibiting SG assembly during virus infection are not well understood. Rather than being inert structures, recent reports suggest SGs have antiviral properties; the granules concentrate and promote interactions between a number of innate immune activators, their downstream interferon-stimulated genes (RIG-I, PKR, MDA5, and OAS), and their targets (5, 41, 43). For example, pattern recognition receptors like RIG-I are activated upon binding to viral RNAs in SGs, which leads to the stimulation of interferon-related genes (42, 43, 82). Alternatively, recent studies suggest that in the absence of virus infection, SGs can activate innate immune signaling (11, 83, 84). Overexpression of G3BP, which leads to SG assembly, recruits and activates PKR within SGs in a novel manner whereby PKR dimerization and viral RNA are not required. This eventually triggers NF-κB-dependent activation of innate immune responses. Since these inquiries have been limited to mammalian cells and insect cells do not encode PKR and RIG-I, it would be interesting to examine if other atypical antiviral proteins are found in SGs, specifically by interrogating wild-type and mutant R146A CrPV infections. Another possibility is that inhibition of SGs during CrPV infection prevents viral proteins from being sequestered to SGs. We have shown that the nonstructural protein CrPV 3C can be sequestered in SGs under cellular stress (62). Identifying the proteins in SGs, especially in R146A CrPV infection, may gain us insights into the causal relationship between SGs and virus infection.

Besides inhibiting SG assembly and host transcription, CrPV-1A, to our surprise, stimulates 5′-end-dependent translation (Fig. 1). Contrary to the shutoff of host translation in CrPV-infected cells, we discovered that CrPV-1A stimulated 5′-end-dependent translation by 2- to 2.5-fold and was dependent on R146 (Fig. 1D and F). It is possible that these results are an artifact of transfection of an exogenous reporter RNA which may not mirror an endogenous mRNA. Alternatively, it is possible that CrPV infection creates a cytoplasmic environment that allows for translation of newly synthesized RNAs, such as the CrPV RNA. In effect, newly synthesized or introduced RNAs are preferentially translated at the expense of existing mRNAs, whether it be CrPV RNA or transfected RNAs. Precedence for this effect is observed in vesicular stomatitis virus (VSV) infection; stimulation of RNA reporter-dependent translation is observed during VSV infection despite global shutoff of host translation and transcription (85). This idea also suggests that the nuclear history of an mRNA would be subject to translational shutoff, as observed in CrPV infection. It is well established that the nuclear history of an mRNA influences its translatability and subcellular localization (86). Finally, transcriptional shutoff by CrPV-1A and suppression of SGs in CrPV-infected S2 cells would further contribute to a cytoplasmic environment that makes translation factors and ribosomes available for viral translation. It will be interesting to determine whether this strategy of modulating SG assembly is more widespread in other virus infections and cellular stresses.

Viruses express a limited number of proteins to modulate cellular processes and block antiviral responses. Because of the restricted coding capacity, a viral protein can have multifunctional properties that affect different processes. For example, the NS1 protein of influenza A virus mediates the export of influenza viral ribonucleoproteins

from the nucleus to the cytoplasm, modulates antiviral defenses by binding to RIG-I and PKR, and inhibits SG assembly (41, 87–89). Our work demonstrates that CrPV-1A is multifunctional and has at least two independent functions that affect distinct cellular processes. Furthermore, our work suggests that CrPV-1A inhibits SG assembly via a conserved mechanism. This viral strategy illuminates how viruses with limited coding capacity have evolved versatile proteins that can evade antiviral responses and affect host cell processes to facilitate virus infection.

## MATERIALS AND METHODS

**Cell culture.** *Drosophila* S2 cells (Invitrogen) were maintained as described in reference 60. S2 cells are devoid of viruses that are commonly persistently infected in these cells. Virus infection was performed as described in reference 60. HeLa cells (already existing collection in the Jan laboratory) were maintained as described previously (90).

The RinGFP stable cell line (Jan laboratory collection) was generated by transfecting 2 $\mu$g of pAc5.1 RinGFP with 0.2 $\mu$g of pIB (Thermo Fisher) using Xtreme-GENE HP DNA transfection reagent (Roche) into S2 cells ($1.5 \times 10^6$ cells/ml; 6-well plates). Five days after transfection, 125 $\mu$g/ml blasticidin (Thermo Fisher Scientific) was added and maintained until stable cell lines were selected.

**Plasmids.** The *Drosophila* expression vector pAc5.1 (Thermo Fisher Scientific), containing DsRed-HA, CrPV-1A-HA, and CrPV-1A(Δ128)-HA, were generated by molecular approaches. A 3× HA tag was inserted between XbaI and ApaI in frame at the C terminus of the protein. CrPV-1A and CrPV-1A(Δ128) were PCR amplified and cloned into KpnI and XbaI of pAc5.1. The construction of the mono-Fluc and CrPV minigenome reporter was previously described in Kerr et al. (65). pcDNA3 CrPV-1A-HA and pcDNA3 CrPV-1A(R146A)-HA were created by subcloning from pAc5.1. Site-directed mutagenesis was used to generate all scanning alanine mutagenesis clones of CrPV-1A. All plasmids were sequence verified.

The CrPV-3 clone and the CrPV-2(Fluc) replicon were described previously (48, 65).

**Virus preparation.** Cells were transfected with CrPV-3 or CrPV-3(R146A) RNA clone as described in reference 65. Intracellular virus, which was collected from multiple freeze-thawing cycles of the transfected cells, was then used to reinfect naive cells to expand the virus stock, as described previously (60). Viral titer was determined by focus-forming assay (60). For mutant R146A virus, virus preparations were RT-PCR amplified and sequenced to verify that the mutation did not revert.

**Transfection and luciferase assay.** DNA transfections were performed using Xtreme-GENE HP DNA transfection reagent (Roche). One microgram of pAc5.1 expression plasmid was cotransfected with 1 $\mu$g of pAc5.1 mono-Fluc into S2 cells ($1.5 \times 10^6$ cells per ml; 6-well plates) as described by the manufacturer (Roche). Cells were harvested with passive lysis buffer (Promega) at the indicated times and assayed for luciferase activity (Promega) using a microplate luminometer (Centro LB 960; Berthold Technologies).

*In vitro*-transcribed RNAs were transfected (0.5 $\mu$g) (Lipofectamine 2000; Invitrogen) into S2 cells ($1.5 \times 10^6$ cells per ml; 12-well plates) as described by the manufacturer (Invitrogen). Cells were harvested with passive lysis buffer (Promega) 10 h after transfection and assayed for luciferase activity (Promega) using a microplate luminometer (Centro LB 960; Berthold Technologies).

***In vitro* transcription.** T7 RNA polymerase reactions were performed as described previously (91). RNA was capped and polyadenylated (CellScript) and then purified (RNeasy kit; Qiagen), and the integrity of the RNA determined by visualization on an agarose gel. The quantity of the RNA was determined by NanoDrop (Thermo Scientific).

**dsRNA-mediated knockdown.** A fragment of firefly luciferase was PCR amplified using primers (5′-ACTGACTAATACGACTCACTATAGGGAGAACTGCCTGCGTGAGATT-3′ and 5′-ACTGACTAATACGACTCACTATAGGGCACACAGTTCGCCTCTTTGA-3′) that contain T7 promoters. The PCR products were used as templates in *in vitro* transcription reactions using T7 RNA polymerase. dsRNA was purified, and its integrity was verified by denaturing gel analysis. dsRNA (13 mg/million cells) was added and incubated in S2 cells in serum-free Shields and Sang medium for 1 h, followed by the addition of complete Shields and Sang medium. S2 cells were incubated with firefly luciferase dsRNAs for 2 days before RNA transfection and luciferase assay.

**Labeling of newly synthesized transcripts by 4-thiouridine.** After adsorption of the virus (30 min), $5 \times 10^6$ mock- or CrPV-infected S2 cells (MOI of 50) were incubated with 200 $\mu$M 4sU for the indicated times. After labeling, RNA was extracted by TRIzol (Invitrogen).

Biotinylation was adapted from reference 67. The extracted RNA was mixed with biotinylation buffer (10 mM HEPES, pH 7.5, 1 mM EDTA) and heated to 65°C for 2 min. Subsequently, 5 $\mu$g of methanethiosulfonate (MTS)-biotin (MTSEA; Biotium) was added to the mixture and incubated for 30 min at room temperature in the dark. The RNA was phenol-chloroform extracted and enriched by ethanol precipitation. Blotting of 4sU-labeled RNA was detected by blotting using Streptavidin-HRP-conjugated antibody. Specifically, RNA was loaded onto a 1% denaturing agarose gel (1× morpholinepropanesulfonic acid [MOPS] and 20%, vol/vol, formaldehyde), transferred, and cross-linked to a nylon membrane (UV Stratalinker 1800; Stratagene). Transfer of RNA was confirmed by methylene blue staining. The membrane was blocked with SDS buffer (1× PBS, 10% SDS, 1 mM EDTA) for 30 min at room temperature. Subsequently, the membrane was probed with Streptavidin-HRP (1:15,000) in 1× PBS and 10% SDS and detected by ECL (Santa Cruz Biotechnology).

Streptavidin pulldown of biotinylated RNAs was performed as described in reference 67. Briefly, Dynabeads MyOne Streptavidin (Invitrogen) beads were blocked with yeast tRNA at a ratio of 5 $\mu$l to 1 $\mu$g for 20 min at room temperature. The beads were washed with high-salt wash buffer (1 M NaCl, 10

mM EDTA, 10 mM Tris-HCl, pH 7.8) 3 times. The beads were then incubated with input RNA at a ratio of 1 $\mu$l to 80 ng in 0.1× high-salt wash buffer for 15 min in the dark with constant agitation. The flowthrough was collected, and the beads were washed 3 times at 65°C and 3 times at room temperature with high-salt wash buffer. RNA was eluted twice upon consecutive addition of 50 $\mu$l and 25 $\mu$l of dithiothreitol (DTT) and enriched by ethanol precipitation. RT-PCR and real-time PCR were performed using primers that were optimized according to MIQE guidelines.

**Radioactive pulse labeling in S2 cells.** S2 cells ($3 \times 10^6$) were pulse labeled with 250 $\mu$Ci [$^{35}$S]Met/Cys (Perkin-Elmer)/ml for 20 min, washed with cold PBS twice, and harvested with 50 $\mu$l modified radioimmunoprecipitation assay (RIPA) buffer (150 mM NaCl, 1% Triton X-100, 1% Nonidet P-40, 0.5% sodium deoxycholate, 0.1% SDS, 50 mM Tris [pH 8.0], and a protease inhibitor cocktail [Roche]). Equal amounts of lysates as determined by Bradford assay were resolved on SDS-PAGE, which was dried and imaged with a phosphorimager (Amersham Pharmacia Biotech).

**Western blot analysis.** S2 cells ($5 \times 10^6$) were lysed in 50 $\mu$l modified RIPA buffer (150 mM NaCl, 1% Triton X-100, 1% Nonidet P-40, 0.5% sodium deoxycholate, 0.1% SDS, 50 mM Tris [pH 8.0], and a protease inhibitor cocktail [Roche]). Equal amounts (in micrograms) of lysates were separated by SDS-PAGE. After transfer to polyvinylidene difluoride (PVDF; Millipore), the membrane was blocked for 30 min in 20 ml of 5% skim milk in TBS-T (20 mM Tris, 150 mM NaCl, 0.1% Tween) and incubated at 4°C overnight with the antibodies mouse $\alpha$-tubulin (1:1,000 dilution; Santa Cruz), mouse $\alpha$-HA (1:500 dilution; Covance), rabbit $\alpha$-CrPV VP2 antibody (1:10,000 dilution; PL Laboratories), rabbit $\alpha$-CrPV RdRp antibody (1:10,000 dilution; PL Laboratories), and mouse $\alpha$-CrPV-1A antibody (1:500 dilution; GenScript) in 5 ml of 5% skim milk in TBS-T. After secondary antibody incubation, the proteins were detected by ECL (Santa Cruz Biotechnology).

**Northern blot analysis.** Total RNA from cells was purified using TRIzol (Invitrogen). Five micrograms of each sample was loaded onto a 1% denaturing agarose gel (1× MOPS and 20%, vol/vol, formaldehyde). RNA was transferred and cross-linked to a nylon membrane (UV Stratalinker 1800; Stratagene). Transfer of RNA was confirmed by methylene blue staining. Northern blotting was performed as described previously (60).

**Immunofluorescence and *in situ* hybridization.** HeLa cells were transferred to coverslips overnight. S2 cells were transferred to coverslips precoated with 0.5 mg/ml concanavalin A (Calbiochem) for 1 h. Subsequently, the cells were fixed with 3% paraformaldehyde in PBS and permeabilized with PBS-T in 3% bovine serum albumin (BSA) (2% Triton X-100). After fixation and permeabilization, the samples are ready for *in situ* hybridization and immunofluorescence.

In preparation for *in situ* hybridization, the coverslips were incubated in hybridization buffer (2× SSC [1× SSC is 0.15 M NaCl plus 0.015 M sodium citrate], 20% formamide, 0.2% BSA, 1 $\mu$g/$\mu$l yeast tRNA) for 15 min at 37°C. Subsequently, the coverslips were hybridized with 1 mg/ml oligo(dT) (40) conjugated to Cy5 (IDT) overnight at 46°C in hybridization buffer. The next day, the cells were washed with 2× SSC with 20% formamide twice for 5 min each at 37°C, 2× SSC twice for 5 min each at 37°C, and 1× SSC once for 5 min. The coverslips were mounted on slides with Prolong Gold antifade reagent (Invitrogen).

Permeabilized cells were washed with 2 ml PBS and incubated with antibodies in 50 $\mu$l PBS containing 5% BSA for 1 h at 25°C. The antibodies used were 1:500 anti-dsRNA (English & Scientific Consulting LLC), 1:500 mouse anti-HA (Covance), 1:500 mouse anti-G3BP (BD Transduction Science), and 1:200 mouse anti-G3BP (Abcam). Cells were subsequently washed with 2 ml PBS three times and incubated with 50 $\mu$l PBS containing appropriate secondary antibodies for 1 h at 25°C. Cells were then washed twice with 2 ml PBS, stained with Hoechst dye (1:20,000 in PBS) for 10 min, and washed once more with 2 ml PBS. Coverslips were mounted on slides with Prolong Gold antifade reagent (Invitrogen). All images except for that shown in Fig. 10A were acquired by a confocal microscope (Olympus FV1000 using Olympus Fluoview Ver.2.0a) with a 60× oil immersion lens. Images shown are a representative single z-section. Photoshop CS6 software was used to process the images. For Fig. 10A, images were acquired by a Deltavision RT microscope with a 100× objective lens (Applied Biosystems). Images shown are z-stacked, and ImageJ with FIJI plugin and Photoshop CS2 were used to process these images.

RinGFP and G3BP foci were manually counted by using a qualitatively determined threshold intensity using ImageJ software (92). Box plots (GraphPad Prism) were used to represent the data.

**Fly stocks and injections.** Isogenic $w^{1118}$ flies were maintained on standard cornmeal food at 25°C and 70% humidity with a 12-h light-dark cycle. Freshly eclosed virgin males and females (10 each) were injected intrathoracically with 200 nl of PBS, CrPV-3, or CrPV-3(R146A) (5,000 FFU) using a PV830 Pneumatic PicoPump (World Precision Instruments) and transferred to standard food. Mortality was monitored daily.

## ACKNOWLEDGMENTS

We thank Raul Andino for critical readings and discussions. We thank Jerry Pelletier for generously providing pateamine A. We acknowledge the UBC Life Sciences Institute Cell Imaging Core Facility for confocal microscopy use and Roy Parker's laboratory (University of Colorado–Boulder) for Deltavision microscope use.

This study was supported by a CIHR operating grant (MOP-81244) to E.J. and an NSERC CGS D Graduate Fellowship to A.K. and C.K.

## REFERENCES


1. Protter DS, Parker R. 2016. Principles and properties of stress granules. Trends Cell Biol 26:668–679. https://doi.org/10.1016/j.tcb.2016.05.004.
2. Arimoto K, Fukuda H, Imajoh-Ohmi S, Saito H, Takekawa M. 2008. Formation of stress granules inhibits apoptosis by suppressing stress-responsive MAPK pathways. Nat Cell Biol 10:1324–1332. https://doi.org/10.1038/ncb1791.
3. Thedieck K, Holzwarth B, Prentzell MT, Boehlke C, Klasener K, Ruf S, Sonntag AG, Maerz L, Grellscheid SN, Kremmer E, Nitschke R, Kuehn EW, Jonker JW, Groen AK, Reth M, Hall MN, Baumeister R. 2013. Inhibition of mTORC1 by astrin and stress granules prevents apoptosis in cancer cells. Cell 154:859–874. https://doi.org/10.1016/j.cell.2013.07.031.
4. Wippich F, Bodenmiller B, Trajkovska MG, Wanka S, Aebersold R, Pelkmans L. 2013. Dual specificity kinase DYRK3 couples stress granule condensation/dissolution to mTORC1 signaling. Cell 152:791–805. https://doi.org/10.1016/j.cell.2013.01.033.
5. Lloyd RE. 2016. Enterovirus control of translation and RNA granule stress responses. Viruses 8:93. https://doi.org/10.3390/v8040093.
6. Onomoto K, Yoneyama M, Fung G, Kato H, Fujita T. 2014. Antiviral innate immunity and stress granule responses. Trends Immunol 35:420–428. https://doi.org/10.1016/j.it.2014.07.006.
7. Kedersha N, Chen S, Gilks N, Li W, Miller IJ, Stahl J, Anderson P. 2002. Evidence that ternary complex (eIF2-GTP-tRNA(i) (Met))-deficient preinitiation complexes are core constituents of mammalian stress granules. Mol Biol Cell 13:195–210. https://doi.org/10.1091/mbc.01-05-0221.
8. Kedersha NL, Gupta M, Li W, Miller I, Anderson P. 1999. RNA-binding proteins TIA-1 and TIAR link the phosphorylation of eIF-2 alpha to the assembly of mammalian stress granules. J Cell Biol 147:1431–1442. https://doi.org/10.1083/jcb.147.7.1431.
9. Dang Y, Kedersha N, Low WK, Romo D, Gorospe M, Kaufman R, Anderson P, Liu JO. 2006. Eukaryotic initiation factor 2alpha-independent pathway of stress granule induction by the natural product pateamine A. J Biol Chem 281:32870–32878. https://doi.org/10.1074/jbc.M606149200.
10. Mazroui R, Sukarieh R, Bordeleau ME, Kaufman RJ, Northcote P, Tanaka J, Gallouzi I, Pelletier J. 2006. Inhibition of ribosome recruitment induces stress granule formation independently of eukaryotic initiation factor 2alpha phosphorylation. Mol Biol Cell 17:4212–4219. https://doi.org/10.1091/mbc.E06-04-0318.
11. Reineke LC, Dougherty JD, Pierre P, Lloyd RE. 2012. Large G3BP-induced granules trigger eIF2alpha phosphorylation. Mol Biol Cell 23:3499–3510. https://doi.org/10.1091/mbc.E12-05-0385.
12. Cherkasov V, Grousl T, Theer P, Vainshtein Y, Glasser C, Mongis C, Kramer G, Stoecklin G, Knop M, Mogk A, Bukau B. 2015. Systemic control of protein synthesis through sequestration of translation and ribosome biogenesis factors during severe heat stress. FEBS Lett 589:3654–3664. https://doi.org/10.1016/j.febslet.2015.10.010.
13. Jain S, Wheeler JR, Walters RW, Agrawal A, Barsic A, Parker R. 2016. ATPase-modulated stress granules contain a diverse proteome and substructure. Cell 164:487–498. https://doi.org/10.1016/j.cell.2015.12.038.
14. Wallace EW, Kear-Scott JL, Pilipenko EV, Schwartz MH, Laskowski PR, Rojek AE, Katanski CD, Riback JA, Dion MF, Franks AM, Airoldi EM, Pan T, Budnik BA, Drummond DA. 2015. Reversible, specific, active aggregates of endogenous proteins assemble upon heat stress. Cell 162:1286–1298. https://doi.org/10.1016/j.cell.2015.08.041.
15. Ohn T, Kedersha N, Hickman T, Tisdale S, Anderson P. 2008. A functional RNAi screen links O-GlcNAc modification of ribosomal proteins to stress granule and processing body assembly. Nat Cell Biol 10:1224–1231. https://doi.org/10.1038/ncb1783.
16. Kedersha N, Cho MR, Li W, Yacono PW, Chen S, Gilks N, Golan DE, Anderson P. 2000. Dynamic shuttling of TIA-1 accompanies the recruitment of mRNA to mammalian stress granules. J Cell Biol 151:1257–1268. https://doi.org/10.1083/jcb.151.6.1257.
17. Tourriere H, Chebli K, Zekri L, Courselaud B, Blanchard JM, Bertrand E, Tazi J. 2003. The RasGAP-associated endoribonuclease G3BP assembles stress granules. J Cell Biol 160:823–831. https://doi.org/10.1083/jcb.200212128.
18. Kedersha N, Ivanov P, Anderson P. 2013. Stress granules and cell signaling: more than just a passing phase? Trends Biochem Sci 38:494–506. https://doi.org/10.1016/j.tibs.2013.07.004.
19. Goulet I, Boisvenue S, Mokas S, Mazroui R, Cote J. 2008. TDRD3, a novel Tudor domain-containing protein, localizes to cytoplasmic stress granules. Hum Mol Genet 17:3055–3074. https://doi.org/10.1093/hmg/ddn203.
20. Chernov KG, Barbet A, Hamon L, Ovchinnikov LP, Curmi PA, Pastre D. 2009. Role of microtubules in stress granule assembly: microtubule dynamical instability favors the formation of micrometric stress granules in cells. J Biol Chem 284:36569–36580. https://doi.org/10.1074/jbc.M109.042879.
21. Loschi M, Leishman CC, Berardone N, Boccaccio GL. 2009. Dynein and kinesin regulate stress-granule and P-body dynamics. J Cell Sci 122:3973–3982. https://doi.org/10.1242/jcs.051383.
22. Buchan JR, Kolaitis RM, Taylor JP, Parker R. 2013. Eukaryotic stress granules are cleared by autophagy and Cdc48/VCP function. Cell 153:1461–1474. https://doi.org/10.1016/j.cell.2013.05.037.
23. Cherkasov V, Hofmann S, Druffel-Augustin S, Mogk A, Tyedmers J, Stoecklin G, Bukau B. 2013. Coordination of translational control and protein homeostasis during severe heat stress. Curr Biol 23:2452–2462. https://doi.org/10.1016/j.cub.2013.09.058.
24. Hilliker A, Gao Z, Jankowsky E, Parker R. 2011. The DEAD-box protein Ded1 modulates translation by the formation and resolution of an eIF4F-mRNA complex. Mol Cell 43:962–972. https://doi.org/10.1016/j.molcel.2011.08.008.
25. Kroschwald S, Maharana S, Mateju D, Malinovska L, Nuske E, Poser I, Richter D, Alberti S. 2015. Promiscuous interactions and protein disaggregases determine the material state of stress-inducible RNP granules. eLife 4:e06807.
26. Yang X, Shen Y, Garre E, Hao X, Krumlinde D, Cvijovic M, Arens C, Nystrom T, Liu B, Sunnerhagen P. 2014. Stress granule-defective mutants deregulate stress responsive transcripts. PLoS Genet 10:e1004763. https://doi.org/10.1371/journal.pgen.1004763.
27. Kedersha N, Stoecklin G, Ayodele M, Yacono P, Lykke-Andersen J, Fritzler MJ, Scheuner D, Kaufman RJ, Golan DE, Anderson P. 2005. Stress granules and processing bodies are dynamically linked sites of mRNP remodeling. J Cell Biol 169:871–884. https://doi.org/10.1083/jcb.200502088.
28. Mollet S, Cougot N, Wilczynska A, Dautry F, Kress M, Bertrand E, Weil D. 2008. Translationally repressed mRNA transiently cycles through stress granules during stress. Mol Biol Cell 19:4469–4479. https://doi.org/10.1091/mbc.E08-05-0499.
29. Fujimura K, Kano F, Murata M. 2008. Identification of PCBP2, a facilitator of IRES-mediated translation, as a novel constituent of stress granules and processing bodies. RNA 14:425–431. https://doi.org/10.1261/rna.780708.
30. Guil S, Long JC, Caceres JF. 2006. hnRNP A1 relocalization to the stress granules reflects a role in the stress response. Mol Cell Biol 26:5744–5758. https://doi.org/10.1128/MCB.00224-06.
31. Lin Y, Protter DS, Rosen MK, Parker R. 2015. Formation and maturation of phase-separated liquid droplets by RNA-binding proteins. Mol Cell 60:208–219. https://doi.org/10.1016/j.molcel.2015.08.018.
32. Molliex A, Temirov J, Lee J, Coughlin M, Kanagaraj AP, Kim HJ, Mittag T, Taylor JP. 2015. Phase separation by low complexity domains promotes stress granule assembly and drives pathological fibrillization. Cell 163:123–133. https://doi.org/10.1016/j.cell.2015.09.015.
33. Poblete-Duran N, Prades-Perez Y, Vera-Otarola J, Soto-Rifo R, Valiente-Echeverria F. 2016. Who regulates whom? An overview of RNA granules and viral infections. Viruses 8:E180.
34. Reineke LC, Lloyd RE. 2013. Diversion of stress granules and P-bodies during viral infection. Virology 436:255–267. https://doi.org/10.1016/j.virol.2012.11.017.
35. Tsai WC, Lloyd RE. 2014. Cytoplasmic RNA granules and viral infection. Annu Rev Virol 1:147–170. https://doi.org/10.1146/annurev-virology-031413-085505.
36. White JP, Cardenas AM, Marissen WE, Lloyd RE. 2007. Inhibition of cytoplasmic mRNA stress granule formation by a viral proteinase. Cell Host Microbe 2:295–305. https://doi.org/10.1016/j.chom.2007.08.006.
37. Cristea IM, Rozjabek H, Molloy KR, Karki S, White LL, Rice CM, Rout MP, Chait BT, MacDonald MR. 2010. Host factors associated with the Sindbis virus RNA-dependent RNA polymerase: role for G3BP1 and G3BP2 in virus replication. J Virol 84:6720–6732. https://doi.org/10.1128/JVI.01983-09.
38. Emara MM, Brinton MA. 2007. Interaction of TIA-1/TIAR with West Nile and dengue virus products in infected cells interferes with stress granule formation and processing body assembly. Proc Natl Acad Sci U S A 104:9041–9046. https://doi.org/10.1073/pnas.0703348104.
39. Fros JJ, Domeradzka NE, Baggen J, Geertsema C, Flipse J, Vlak JM, Pijlman GP. 2012. Chikungunya virus nsP3 blocks stress granule assembly by recruitment of G3BP into cytoplasmic foci. J Virol 86:10873–10879. https://doi.org/10.1128/JVI.01506-12.

40. Panas MD, Varjak M, Lulla A, Eng Merits KEA, Karlsson Hedestam GB, McInerney GM. 2012. Sequestration of G3BP coupled with efficient translation inhibits stress granules in Semliki Forest virus infection. Mol Biol Cell 23:4701–4712. https://doi.org/10.1091/mbc.E12-08-0619.
41. Khaperskyy DA, Hatchette TF, McCormick C. 2012. Influenza A virus inhibits cytoplasmic stress granule formation. FASEB J 26:1629–1639. https://doi.org/10.1096/fj.11-196915.
42. Oh SW, Onomoto K, Wakimoto M, Onoguchi K, Ishidate F, Fujiwara T, Yoneyama M, Kato H, Fujita T. 2016. Leader-containing uncapped viral transcript activates RIG-I in antiviral stress granules. PLoS Pathog 12: e1005444. https://doi.org/10.1371/journal.ppat.1005444.
43. Onomoto K, Jogi M, Yoo JS, Narita R, Morimoto S, Takemura A, Sambhara S, Kawaguchi A, Osari S, Nagata K, Matsumiya T, Namiki H, Yoneyama M, Fujita T. 2012. Critical role of an antiviral stress granule containing RIG-I and PKR in viral detection and innate immunity. PLoS One 7:e43031. https://doi.org/10.1371/journal.pone.0043031.
44. Bonning BC, Miller WA. 2010. Dicistroviruses. Annu Rev Entomol 55: 129–150. https://doi.org/10.1146/annurev-ento-112408-085457.
45. Cox-Foster DL, Conlan S, Holmes EC, Palacios G, Evans JD, Moran NA, Quan PL, Briese T, Hornig M, Geiser DM, Martinson V, van Engelsdorp D, Kalkstein AL, Drysdale A, Hui J, Zhai J, Cui L, Hutchison SK, Simons JF, Egholm M, Pettis JS, Lipkin WI. 2007. A metagenomic survey of microbes in honey bee colony collapse disorder. Science 318:283–287. https://doi.org/10.1126/science.1146498.
46. Lightner DV. 1996. Epizootiology, distribution and the impact on international trade of two penaeid shrimp viruses in the Americas. Rev Sci Tech 15:579–601.
47. Lightner DV, Redman RM, Poulos BT, Nunan LM, Mari JL, Hasson KW. 1997. Risk of spread of penaeid shrimp viruses in the Americas by the international movement of live and frozen shrimp. Rev Sci Tech 16: 146–160.
48. Khong A, Bonderoff JM, Spriggs RV, Tammpere E, Kerr CH, Jackson TJ, Willis AE, Jan E. 2016. Temporal regulation of distinct internal ribosome entry sites of the dicistroviridae cricket paralysis virus. Viruses 8:E25.
49. Wilson JE, Powell MJ, Hoover SE, Sarnow P. 2000. Naturally occurring dicistronic cricket paralysis virus RNA is regulated by two internal ribosome entry sites. Mol Cell Biol 20:4990–4999. https://doi.org/10.1128/MCB.20.14.4990-4999.2000.
50. Kemp C, Mueller S, Goto A, Barbier V, Paro S, Bonnay F, Dostert C, Troxler L, Hetru C, Meignin C, Pfeffer S, Hoffmann JA, Imler JL. 2013. Broad RNA interference-mediated antiviral immunity and virus-specific inducible responses in Drosophila. J Immunol 190:650–658. https://doi.org/10.4049/jimmunol.1102486.
51. Dostert C, Jouanguy E, Irving P, Troxler L, Galiana-Arnoux D, Hetru C, Hoffmann JA, Imler JL. 2005. The Jak-STAT signaling pathway is required but not sufficient for the antiviral response of drosophila. Nat Immunol 6:946–953. https://doi.org/10.1038/ni1237.
52. Nayak A, Berry B, Tassetto M, Kunitomi M, Acevedo A, Deng C, Krutchinsky A, Gross J, Antoniewski C, Andino R. 2010. Cricket paralysis virus antagonizes Argonaute 2 to modulate antiviral defense in Drosophila. Nat Struct Mol Biol 17:547–554. https://doi.org/10.1038/nsmb.1810.
53. van Rij RP, Saleh MC, Berry B, Foo C, Houk A, Antoniewski C, Andino R. 2006. The RNA silencing endonuclease Argonaute 2 mediates specific antiviral immunity in Drosophila melanogaster. Genes Dev 20: 2985–2995. https://doi.org/10.1101/gad.1482006.
54. Costa A, Jan E, Sarnow P, Schneider D. 2009. The Imd pathway is involved in antiviral immune responses in Drosophila. PLoS One 4:e7436. https://doi.org/10.1371/journal.pone.0007436.
55. Cherry S, Doukas T, Armknecht S, Whelan S, Wang H, Sarnow P, Perrimon N. 2005. Genome-wide RNAi screen reveals a specific sensitivity of IRES-containing RNA viruses to host translation inhibition. Genes Dev 19:445–452. https://doi.org/10.1101/gad.1267905.
56. Cherry S, Kunte A, Wang H, Coyne C, Rawson RB, Perrimon N. 2006. COPI activity coupled with fatty acid biosynthesis is required for viral replication. PLoS Pathog 2:e102. https://doi.org/10.1371/journal.ppat.0020102.
57. Merkling SH, Bronkhorst AW, Kramer JM, Overheul GJ, Schenck A, Van Rij RP. 2015. The epigenetic regulator G9a mediates tolerance to RNA virus infection in Drosophila. PLoS Pathog 11:e1004692. https://doi.org/10.1371/journal.ppat.1004692.
58. Merkling SH, Overheul GJ, van Mierlo JT, Arends D, Gilissen C, van Rij RP. 2015. The heat shock response restricts virus infection in Drosophila. Sci Rep 5:12758. https://doi.org/10.1038/srep12758.
59. Wu X, He WT, Tian S, Meng D, Li Y, Chen W, Li L, Tian L, Zhong CQ, Han F, Chen J, Han J. 2014. pelo is required for high efficiency viral replication. PLoS Pathog 10:e1004034. https://doi.org/10.1371/journal.ppat.1004034.
60. Garrey JL, Lee YY, Au HH, Bushell M, Jan E. 2010. Host and viral translational mechanisms during cricket paralysis virus infection. J Virol 84:1124–1138. https://doi.org/10.1128/JVI.02006-09.
61. Moore NF, Kearns A, Pullin JS. 1980. Characterization of cricket paralysis virus-induced polypeptides in Drosophila cells. J Virol 33:1–9.
62. Khong A, Jan E. 2011. Modulation of stress granules and P bodies during dicistrovirus infection. J Virol 85:1439–1451. https://doi.org/10.1128/JVI.02220-10.
63. Wang XH, Aliyari R, Li WX, Li HW, Kim K, Carthew R, Atkinson P, Ding SW. 2006. RNA interference directs innate immunity against viruses in adult Drosophila. Science 312:452–454. https://doi.org/10.1126/science.1125694.
64. Chtarbanova S, Lamiable O, Lee KZ, Galiana D, Troxler L, Meignin C, Hetru C, Hoffmann JA, Daeffler L, Imler JL. 2014. Drosophila C virus systemic infection leads to intestinal obstruction. J Virol 88: 14057–14069. https://doi.org/10.1128/JVI.02320-14.
65. Kerr CH, Wang QS, Keatings K, Khong A, Allan D, Yip CK, Foster LJ, Jan E. 2015. The 5′ untranslated region of a novel infectious molecular clone of the dicistrovirus cricket paralysis virus modulates infection. J Virol 89: 5919–5934. https://doi.org/10.1128/JVI.00463-15.
66. Doukas T, Sarnow P. 2011. Escape from transcriptional shutoff during poliovirus infection: NF-kappaB-responsive genes IkappaBa and A20. J Virol 85:10101–10108. https://doi.org/10.1128/JVI.00575-11.
67. Duffy EE, Rutenberg-Schoenberg M, Stark CD, Kitchen RR, Gerstein MB, Simon MD. 2015. Tracking distinct RNA populations using efficient and reversible covalent chemistry. Mol Cell 59:858–866. https://doi.org/10.1016/j.molcel.2015.07.023.
68. Irvine K, Stirling R, Hume D, Kennedy D. 2004. Rasputin, more promiscuous than ever: a review of G3BP. Int J Dev Biol 48:1065–1077. https://doi.org/10.1387/ijdb.041893ki.
69. Bordeleau ME, Matthews J, Wojnar JM, Lindqvist L, Novac O, Jankowsky E, Sonenberg N, Northcote P, Teesdale-Spittle P, Pelletier J. 2005. Stimulation of mammalian translation initiation factor eIF4A activity by a small molecule inhibitor of eukaryotic translation. Proc Natl Acad Sci U S A 102:10460–10465. https://doi.org/10.1073/pnas.0504249102.
70. Weber F, Wagner V, Rasmussen SB, Hartmann R, Paludan SR. 2006. Double-stranded RNA is produced by positive-strand RNA viruses and DNA viruses but not in detectable amounts by negative-strand RNA viruses. J Virol 80:5059–5064. https://doi.org/10.1128/JVI.80.10.5059-5064.2006.
71. Buchan JR, Parker R. 2009. Eukaryotic stress granules: the ins and outs of translation. Mol Cell 36:932–941. https://doi.org/10.1016/j.molcel.2009.11.020.
72. Fros JJ, Pijlman GP. 2016. Alphavirus infection: host cell shut-off and inhibition of antiviral responses. Viruses 8:E166.
73. Lin JY, Chen TC, Weng KF, Chang SC, Chen LL, Shih SR. 2009. Viral and host proteins involved in picornavirus life cycle. J Biomed Sci 16:103. https://doi.org/10.1186/1423-0127-16-103.
74. Rivas HG, Schmaling SK, Gaglia MM. 2016. Shutoff of host gene expression in influenza A virus and herpesviruses: similar mechanisms and common themes. Viruses 8:102. https://doi.org/10.3390/v8040102.
75. Imler JL. 2014. Overview of Drosophila immunity: a historical perspective. Dev Comp Immunol 42:3–15. https://doi.org/10.1016/j.dci.2013.08.018.
76. Merkling SH, van Rij RP. 2013. Beyond RNAi: antiviral defense strategies in Drosophila and mosquito. J Insect Physiol 59:159–170. https://doi.org/10.1016/j.jinsphys.2012.07.004.
77. Zhu F, Ding H, Zhu B. 2013. Transcriptional profiling of Drosophila S2 cells in early response to Drosophila C virus. Virol J 10:210. https://doi.org/10.1186/1743-422X-10-210.
78. Guo L, Shorter J. 2015. It's raining liquids: RNA tunes viscoelasticity and dynamics of membraneless organelles. Mol Cell 60:189–192. https://doi.org/10.1016/j.molcel.2015.10.006.
79. Zhang H, Elbaum-Garfinkle S, Langdon EM, Taylor N, Occhipinti P, Bridges AA, Brangwynne CP, Gladfelter AS. 2015. RNA controls polyQ protein phase transitions. Mol Cell 60:220–230. https://doi.org/10.1016/j.molcel.2015.09.017.
80. Khaperskyy DA, Emara MM, Johnston BP, Anderson P, Hatchette TF, McCormick C. 2014. Influenza a virus host shutoff disables antiviral stress-induced translation arrest. PLoS Pathog 10:e1004217. https://doi.org/10.1371/journal.ppat.1004217.
81. Piotrowska J, Hansen SJ, Park N, Jamka K, Sarnow P, Gustin KE. 2010. Stable

formation of compositionally unique stress granules in virus-infected cells. J Virol 84:3654–3665. https://doi.org/10.1128/JVI.01320-09.
82. Yoo JS, Takahasi K, Ng CS, Ouda R, Onomoto K, Yoneyama M, Lai JC, Lattmann S, Nagamine Y, Matsui T, Iwabuchi K, Kato H, Fujita T. 2014. DHX36 enhances RIG-I signaling by facilitating PKR-mediated antiviral stress granule formation. PLoS Pathog 10:e1004012. https://doi.org/10.1371/journal.ppat.1004012.
83. Reineke LC, Kedersha N, Langereis MA, van Kuppeveld FJ, Lloyd RE. 2015. Stress granules regulate double-stranded RNA-dependent protein kinase activation through a complex containing G3BP1 and Caprin1. mBio 6:e02486.
84. Reineke LC, Lloyd RE. 2015. The stress granule protein G3BP1 recruits protein kinase R to promote multiple innate immune antiviral responses. J Virol 89:2575–2589. https://doi.org/10.1128/JVI.02791-14.
85. Whitlow ZW, Connor JH, Lyles DS. 2006. Preferential translation of vesicular stomatitis virus mRNAs is conferred by transcription from the viral genome. J Virol 80:11733–11742. https://doi.org/10.1128/JVI.00971-06.
86. Giorgi C, Moore MJ. 2007. The nuclear nurture and cytoplasmic nature of localized mRNPs. Semin Cell Dev Biol 18:186–193. https://doi.org/10.1016/j.semcdb.2007.01.002.
87. York A, Fodor E. 2013. Biogenesis, assembly, and export of viral messenger ribonucleoproteins in the influenza A virus infected cell. RNA Biol 10:1274–1282. https://doi.org/10.4161/rna.25356.
88. Mibayashi M, Martinez-Sobrido L, Loo YM, Cardenas WB, Gale M, Jr, Garcia-Sastre A. 2007. Inhibition of retinoic acid-inducible gene I-mediated induction of beta interferon by the NS1 protein of influenza A virus. J Virol 81:514–524. https://doi.org/10.1128/JVI.01265-06.
89. Li S, Min JY, Krug RM, Sen GC. 2006. Binding of the influenza A virus NS1 protein to PKR mediates the inhibition of its activation by either PACT or double-stranded RNA. Virology 349:13–21. https://doi.org/10.1016/j.virol.2006.01.005.
90. Jagdeo JM, Dufour A, Fung G, Luo H, Kleifeld O, Overall CM, Jan E. 2015. Heterogeneous nuclear ribonucleoprotein M facilitates enterovirus infection. J Virol 89:7064–7078. https://doi.org/10.1128/JVI.02977-14.
91. Wang QS, Jan E. 2014. Switch from cap- to factorless IRES-dependent 0 and +1 frame translation during cellular stress and dicistrovirus infection. PLoS One 9:e103601. https://doi.org/10.1371/journal.pone.0103601.
92. Schneider CA, Rasband WS, Eliceiri KW. 2012. NIH Image to ImageJ: 25 years of image analysis. Nat Methods 9:671–675. https://doi.org/10.1038/nmeth.2089.